

# Two-Photon Physics in Hadronic Processes

Carl E. Carlson

Department of Physics

College of William and Mary, Williamsburg, Virginia 23187

and

Marc Vanderhaeghen

Thomas Jefferson National Accelerator Facility

Newport News, VA 23606

and

Department of Physics

College of William and Mary, Williamsburg, Virginia 23187

31 January 2007

KEY WORDS:

electron scattering, form factors, two-photon exchange processes

---

## Abstract

Two-photon exchange contributions to elastic electron-scattering are reviewed. The apparent discrepancy in the extraction of elastic nucleon form factors between unpolarized Rosenbluth and polarization transfer experiments is discussed, as well as the understanding of this puzzle in terms of two-photon exchange corrections. Calculations of such corrections both within partonic and hadronic frameworks are reviewed. In view of recent spin-dependent electron scattering data, the relation of the two-photon exchange process to the hyperfine splitting in hydrogen is critically examined. The imaginary part of the two-photon exchange amplitude as can be accessed from the beam normal spin asymmetry in elastic electron-nucleon scattering is reviewed. Further extensions and open issues in this field are outlined.

---

I like a thing simple but it must be simple through complication. Everything must come into your scheme, otherwise you cannot achieve real simplicity.

Gertrude Stein, “Afterword,” *What Are Masterpieces*

# Contents

<b>1</b>	<b>Introduction</b>	<b>3</b>
<b>2</b>	<b>Two-photon in elastic electron-nucleon scattering</b>	<b>7</b>
2.1	Hard two-photon exchange . . . . .	7
2.2	Elastic electron-nucleon scattering observables . . . . .	8
2.3	Two-photon exchange at the quark level . . . . .	9
2.4	Calculation using generalized parton distributions . . . . .	11
2.5	Results . . . . .	13
2.5.1	Cross section . . . . .	13
2.5.2	Polarization transfers . . . . .	14
2.5.3	Positron-proton vs. electron-proton . . . . .	14
2.5.4	Results from single-baryon intermediate states . . . . .	15
2.6	Remarks on related topics . . . . .	15
<b>3</b>	<b>Polarizability corrections to hydrogen hyperfine splitting</b>	<b>18</b>
3.1	Two-photon exchange and atomic structure . . . . .	18
3.2	Hyperfine splitting calculations . . . . .	18
3.3	Numerics, especially for $\Delta_{\text{pol}}$ . . . . .	21
3.4	Comments on the derivations of the formulas . . . . .	23
3.5	Remarks and prospects . . . . .	25
<b>4</b>	<b>Beam and target normal spin asymmetries</b>	<b>26</b>
4.1	Single spin asymmetries in elastic electron-nucleon scattering . . . . .	27
4.2	Imaginary (absorptive) part of the two-photon exchange amplitude . . . . .	28
4.3	Results and discussion . . . . .	29
4.3.1	Threshold region . . . . .	29
4.3.2	Resonance region . . . . .	29
4.3.3	High-energy, forward scattering (diffractive) region . . . . .	30
4.3.4	Hard scattering region . . . . .	31
<b>5</b>	<b>Conclusions and open issues</b>	<b>34</b>

# 1 Introduction

Elastic electron-nucleon scattering in the one-photon exchange approximation is a time-honored tool to access information on the structure of hadrons. Experiments with increasing precision have become possible in recent years, mainly triggered by new techniques to perform polarization experiments at electron scattering facilities. This opened a new frontier in the measurement of hadron structure quantities, such as its electroweak form factors, parity violating effects, nucleon polarizabilities, transition form factors, or the measurement of spin dependent structure functions, to name a few. For example, experiments using polarized electron beams and measuring the ratio of the recoil nucleon in-plane polarization components have profoundly extended our understanding of the nucleon electromagnetic form factors (FFs); for recent reviews on nucleon FFs see e.g. Refs. [1, 2, 3]. For the proton, such polarization experiments access the ratio  $G_E/G_M$  of the proton's electric (  $G_E$  ) to magnetic (  $G_M$  ) FFs directly from the ratio of the “sideways” and “longitudinal” polarizations in elastic electron-nucleon scattering as [4],

$$\frac{P_s}{P_l} = -\sqrt{\frac{2\varepsilon}{\tau(1+\varepsilon)}} \frac{G_E(Q^2)}{G_M(Q^2)} . \quad (1)$$

Here,

$$\tau \equiv \frac{Q^2}{4M^2} , \quad \frac{1}{\varepsilon} \equiv 1 + 2(1 + \tau) \tan^2 \frac{\theta}{2} , \quad (2)$$

$Q^2 = -q^2$  is the momentum transfer squared,  $\theta$  is the laboratory scattering angle, and  $0 \leq \varepsilon \leq 1$ . Recently, this ratio has been measured at the Jefferson Laboratory out to a space-like momentum transfer  $Q^2$  of 5.6 GeV<sup>2</sup> [5, 6, 7]. It came as a surprise that these experiments extracted a ratio of  $G_E/G_M$  which is clearly at variance with unpolarized measurements [8, 9, 10] using the Rosenbluth separation technique, which measures the angular dependence of the differential cross section for elastic electron-nucleon scattering at fixed  $Q^2$ ,

$$\frac{d\sigma}{d\Omega_{Lab}} \propto G_M^2 + \frac{\varepsilon}{\tau} G_E^2 , \quad (3)$$

where the proportionality factor is well known, and isolates the  $\varepsilon$ -dependent term. In each case, the quoted formulas assume single-photon exchange between electron and nucleon.

To explain the discrepancy between the two experimental techniques, suspicion falls on the Rosenbluth measurements, but not because of experimental problems *per se*. The Rosenbluth formula, Eq. (3), at high  $Q^2$  has a numerically big term,  $G_M^2$ , and a small term. The results for  $G_E$  come from the small term. Any omitted  $\varepsilon$ -dependent corrections to the large term can thus have a strikingly large effect on  $G_E$ .

Two-photon exchange, Fig. 1, is one thinkable culprit. The subject has a long history. In fact as early as the late 1950s and during the 1960s, when electron-nucleon scattering was measured systematically at the Stanford Linear Accelerator Center to access nucleon electromagnetic FFs, the validity of the one-photon exchange approximation has been discussed both theoretically and experimentally. Because the one-photon exchange cross section depends quadratically on the lepton charge, the difference between electron-nucleon and positron-nucleon cross sections is a test for two- or multi-photon exchange processes. Early comparisons of electron- and positron-nucleon scattering cross sections

were consistent with equal cross sections [11, 12], but the precision achieved in those early investigations could not exclude two-photon exchange effects at the few percent level of the cross section. Contributions of this size can be expected due to the additional electromagnetic coupling in the two-photon exchange diagram, which brings in a suppression factor  $\alpha = e^2/(4\pi) \simeq 1/137$ .

On the theory side, the calculation of corrections to elastic electron-nucleon scattering of order  $e^2$  relative to the Born approximation, also known as radiative corrections, have a long history, see *e.g.* Refs. [13, 14], which were heavily applied in the analysis of early electron-nucleon scattering experiments. The infrared divergences associated with one photon in Fig. 1 being soft, *i.e.*, having a vanishingly small four-momentum, had been extracted—they cancel against infrared divergences from soft bremsstrahlung—but the contributions when both photons are hard (*i.e.*, when the momentum transfer of both individual photons is large) were not calculated in those works because of insufficient knowledge of the intermediate hadron state. The early calculators were well aware of the omission, and explicitly expressed hope that the missing contributions would be small. Some early estimates of the two-photon exchange contribution of Fig. 1 with two hard photons were attempted though in the late 1950s by Drell and collaborators [15, 16]. Those works constructed a non-relativistic model for the blob in Fig. 1, including the nucleon and lowest nucleon resonance contribution, the  $\Delta(1232)$ . The calculation found that the resonance contribution to the two-photon exchange diagram affects the cross sections at the  $\sim 1\%$  level. Due to the non-relativistic nature of the calculation, the result was limited to about 1 GeV electron beam energy. In subsequent works, *e.g.* Refs. [17, 18], two-photon exchange effects were approximately calculated to higher energies. In particular, Greenhut [18] evaluated the contribution of higher nucleon resonance intermediate states, with masses up to 1.7 GeV, when evaluating the blob in Fig. 1. It was found that the dispersive (real) part of the two-photon amplitude yields an electron to positron cross section ratio which deviates from unity at the 1-2 % level in the few GeV region. The relative smallness of the resonance contribution partly originates because the real parts of the resonance amplitudes change sign in the integrand entering the evaluation of the box diagram.

Triggered by the experimental discrepancy between polarization transfer and Rosenbluth measurements of the proton form factor ratio  $G_E/G_M$  at larger  $Q^2$  in recent years, the field has seen a new life. In 2003, it was noticed in Ref. [19] that the general form of the two-photon exchange graphs could be expressed in an effective current  $\times$  current form, but with an extra structure beyond those that gave  $G_M$  and  $G_E$ . Further, if this extra term had the size one might estimate from perturbation theory, then its interference with the one-photon exchange amplitude could be comparable in size to the  $(G_E)^2$  term in the

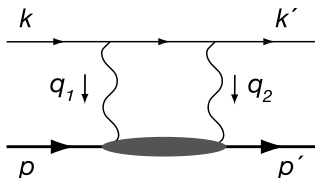


Figure 1: Two photon exchange in the lepton - nucleon scattering process  $l(k) + N(p) \rightarrow l(k') + N(p')$ , with  $k, k'$  ( $p, p'$ ) the four-momenta of leptons (nucleons) respectively.

Rosenbluth cross section at large  $Q^2$ . In addition, there could be  $\varepsilon$ -dependent modifications to the  $(G_M)^2$  term. Hence there was motivation for a precise evaluation. Realistic calculations of elastic electron-nucleon scattering beyond the Born approximation are required in order to demonstrate in a quantitative way that  $2\gamma$  exchange effects are indeed able to resolve this discrepancy at larger  $Q^2$ . In the current work, we will review several such attempts and describe the present status of this field. On the experimental side, recent years have seen first attempts to extract the effect of two-photon exchange contributions in a quantitative way from the electron-proton scattering data [20].

Besides offering a way to explain the glaring discrepancy between two methods of measuring the proton electric form factor, the study of two-photon processes also contain opportunities to access nucleon structure physics which surpasses the information contained in nucleon FFs. The possibility arises because a successful two-photon calculation involving a hadronic system requires knowledge of hadronic structure, of a sort which has only been available recently. For example, one line of investigation arises when the virtuality of one or both of the photons in the two-photon process is large compared to a nucleon mass scale. In that case, the hard scale allows one to access the Compton scattering subprocess on a quark within the nucleon. The new (non-perturbative) pieces of information which one then accesses from such a process are the quark correlation functions within the nucleon, also known as generalized parton distributions (GPDs); for recent reviews see Refs. [21, 22, 23, 24, 25]. We will review how these GPDs can in turn be used to estimate the two-photon exchange diagram of Fig. 1 at large  $Q^2$ .

Another line of calculations involves the hadronic corrections to ultra-high precision atomic physics experiments, such as the hydrogen hyperfine-splitting. Theoretical predictions for quantities such as the Lamb shift in hydrogen or the hydrogen hyperfine splitting can currently be performed within quantum electrodynamics to such accuracy that the leading theoretical uncertainties are related to the nuclear size or the nuclear excitation spectrum; for reviews see e.g. Refs. [26, 27]. For the hyperfine splitting in hydrogen, which is known to 13 significant figures, current theoretical understanding is at the part per million level. The leading theoretical uncertainty involves the calculation of the two-photon exchange graph of Fig. 1 for zero momentum transfer between the bound electron and the proton, allowing for all nucleon excited states in the blob. The current theoretical understanding of these two-photon exchange corrections will be reviewed in this work.

There are several physical problems where a one-photon exchange potential is not sufficiently accurate. Besides the description of simple atoms, such as hydrogen and helium, also for a precise description of positronium one needs to include two- and multi-photon exchange effects. In particular in the interaction of electrically neutral systems, such as neutral atoms and molecules, the effect of two-photon exchange gives the dominant contribution to the forces between such systems, for a theoretical review of such dispersion forces; see *e.g.* Ref. [28].

To push the precision frontier further in electron scattering as well as in the hadronic corrections to atomic physics quantities, one needs a good control of  $2\gamma$  exchange mechanisms and needs to understand how they may or may not affect different observables. This justifies a systematic study of such  $2\gamma$  exchange effects, both theoretically and experimentally. Besides the real (dispersive) part of the  $2\gamma$  exchange amplitude, which can be accessed by reversing the sign of the lepton charge, also precise measurements of the imaginary part of the  $2\gamma$  exchange amplitude became possible in very recent years. The imaginary (absorptive) part of the  $2\gamma$  exchange amplitude can be accessed through a single spin asymmetry (SSA) in elastic electron-nucleon scattering, when either the target

or beam spin are polarized normal to the scattering plane, as has been discussed some time ago [29, 30]. As time reversal invariance forces this SSA to vanish for one-photon exchange, it is of order  $\alpha = e^2/(4\pi) \simeq 1/137$ . Furthermore, to polarize an ultra-relativistic particle in the direction normal to its momentum involves a suppression factor  $m/E$  (with  $m$  the mass and  $E$  the energy of the particle), which typically is of order  $10^{-4} - 10^{-3}$  for the electron when the electron beam energy is in the 1 GeV range. Therefore, the resulting target normal SSA can be expected to be of order  $10^{-2}$ , whereas the beam normal SSA is of order  $10^{-6} - 10^{-5}$ . Measurements of small asymmetries of the order ppm are quite demanding experimentally, but have been performed in very recent years, and will also be reviewed in this work.

The outline of the present work is as follows. In Section 2, we review the elastic electron-nucleon scattering beyond the Born approximation and highlight the discrepancy in the extraction of  $G_E/G_M$  using polarization transfer and unpolarized (Rosenbluth) measurements. We give a brief review of the different attempts which have been made recently to explain this difference in terms of two-photon exchange corrections, and present in more detail a partonic description at larger momentum transfers.

In Section 3, we describe the hadronic corrections of the hydrogen hyperfine splitting, based on the latest evaluation of the forward polarized structure functions which enter in the calculation of the two-photon exchange diagram.

In Section 4, we review the beam and target single spin asymmetries which measure the imaginary part of the two-photon exchange amplitude. In particular, we give an overview of the recent high precision measurements in case of a polarized beam with normal beam spin polarization.

We conclude in Section 5, and spell out a few open issues in this field.

## 2 Two-photon in elastic electron-nucleon scattering

### 2.1 Hard two-photon exchange

In this section, we study attempts to evaluate completely the two-photon exchange contributions to electron-proton elastic scattering, specifically including the exchange of two hard photons, which can probe well inside the proton and which require detailed knowledge of proton structure to evaluate. The immediate motivation, already given in the introduction, is the conflict between the Rosenbluth, with pre-2003 radiative corrections, and the polarization measurements of  $G_E/G_M$  for the proton. The difference between the two techniques is a factor 4 at  $Q^2 = 5.6 \text{ GeV}^2$ ! (The data will appear on plots later in this section, when we discuss how well the proposed resolutions of the conundrum are working.)

Modern quantitative calculations either treat the hadronic intermediate state in Fig. 1 as a proton plus a set of resonances, or else treat it in a constituent picture using generalized parton distributions.

In the earliest of the modern calculations, Blunden, Melnitchouk, and Tjon [31] evaluated the two-photon exchange amplitude keeping just the elastic nucleon intermediate state. They found that the two-photon exchange correction with an intermediate nucleon has the proper sign and magnitude to partially resolve the discrepancy between the two experimental techniques. Later, the same group, joined by Kondratyuk [33], included contributions of the  $\Delta(1232)$  in the intermediate state, which partly canceled the elastic terms. Most recently, Kondratyuk and Blunden [34] included five more baryon resonances in the intermediate state. While finding that the overall contribution of the additional resonances was not large, the totality of their corrections with their choices for the  $\gamma$ -nucleon-resonance vertices leads to good agreement with the Rosenbluth data using the form factors obtained from polarization data.

Borisyuk and Kobushkin [35] also considered two-photon corrections with elastic nucleon intermediate states, and used dispersive techniques to reduce the necessary integrals to ones involving the vertex form factors with only spacelike momentum transfers. They were able to reduce it further to a single numerical integral for sufficiently low  $Q^2$ . (They do not show any Rosenbluth-type plots, but their plotted results for (say)  $\delta G_M/G_M$ , in notation defined below, are in line with results known from what will be described in the rest of this section, despite the rather different methodology.)

In [36, 37], a group including the present authors calculated the hard two-photon elastic electron-nucleon scattering amplitude at large momentum transfers by relating the required virtual Compton process on the nucleon to generalized parton distributions (GPDs), which also enter in other wide angle scattering processes. This approach effectively sums all possible excitations of inelastic nucleon intermediate states. It was found that the two-photon corrections to the Rosenbluth process indeed can substantially reconcile the two ways of measuring  $G_E/G_M$ .

Rosenbluth data is also available where the recoiling proton, rather than the electron, is detected [10]. These data appear to match the data where the scattered electron was detected. The two-photon exchange contributions are the same whatever particle is detected. However, the bremsstrahlung corrections are different. We shall defer detailed discussion of the proton-detected data pending reassessment of the original [14, 38] and the new [39, 10] proton-observed bremsstrahlung calculations.



## 2.2 Elastic electron-nucleon scattering observables

In order to describe elastic electron-nucleon scattering,

$$l(k, h) + N(p, \lambda_N) \rightarrow l(k', h') + N(p', \lambda'_N), \quad (4)$$

where  $h, h', \lambda_N$ , and  $\lambda'_N$  are helicities, we adopt the definitions

$$P = \frac{p + p'}{2}, \quad K = \frac{k + k'}{2}, \quad q = k - k' = p' - p, \quad (5)$$

define the Mandelstam variables

$$s = (p + k)^2, \quad t = q^2 = -Q^2, \quad u = (p - k')^2, \quad (6)$$

let  $\nu \equiv K \cdot P$ , and let  $M$  be the nucleon mass.

The  $T$ -matrix helicity amplitudes are given by

$$T_{\lambda'_N, \lambda_N}^{h', h} \equiv \langle k', h'; p', \lambda'_N | T | k, h; p, \lambda_N \rangle. \quad (7)$$

Parity invariance reduces the number of independent helicity amplitudes from 16 to 8. Time reversal invariance further reduces the number to 6 [40]. Further still, in a gauge theory lepton helicity is conserved to all orders in perturbation theory when the lepton mass is zero. We shall neglect the lepton mass. This finally reduces the number of independent helicity amplitudes to 3, which one may for example choose as

$$T_{+,+}^{+,+}; \quad T_{-,-}^{+,+}; \quad T_{-,+}^{+,+} = T_{+,-}^{+,+}. \quad (8)$$

(The phase in the last equality is for particle momenta in the  $xz$  plane.)

Alternatively, one can expand in terms of a set of three independent Lorentz structures, multiplied by three generalized form factors. One such  $T$ -matrix expansion is

$$\begin{aligned} T_{h, \lambda'_N, \lambda_N} &= \frac{e^2}{Q^2} \bar{u}(k', h) \gamma_\mu u(k, h) \\ &\times \bar{u}(p', \lambda'_N) \left( \tilde{G}_M \gamma^\mu - \tilde{F}_2 \frac{P^\mu}{M} + \tilde{F}_3 \frac{\gamma \cdot K P^\mu}{M^2} \right) u(p, \lambda_N). \end{aligned} \quad (9)$$

The expansion is general. The overall factors and the notations  $\tilde{G}_M$  and  $\tilde{F}_2$  have been chosen [19] to have a straightforward connection to the standard form factors in the one-photon exchange limit.

If desired, one may replace the  $\tilde{F}_3$  term by an axial-like term using the identity,

$$\begin{aligned} \bar{u}(k') \gamma \cdot P u(k) \times \bar{u}(p') \gamma \cdot K u(p) &= \frac{s - u}{4} \bar{u}(k') \gamma_\mu u(k) \times \bar{u}(p') \gamma^\mu u(p) \\ &+ \frac{t}{4} \bar{u}(k') \gamma_\mu \gamma_5 u(k) \times \bar{u}(p') \gamma^\mu \gamma_5 u(p), \end{aligned} \quad (10)$$

which is valid for massless leptons and any nucleon mass. We will, however, continue with the  $T$ -matrix in the form shown in Eq. (9). An equivalent expansion has also been studied in Ref. [41].



The scalar quantities  $\tilde{G}_M$ ,  $\tilde{F}_2$ , and  $\tilde{F}_3$  are complex functions of two variables, say  $\nu$  and  $Q^2$ . We also use

$$\tilde{G}_E \equiv \tilde{G}_M - (1 + \tau)\tilde{F}_2. \quad (11)$$

To separately identify the one- and two-photon exchange contributions, we use the notation  $\tilde{G}_M = G_M + \delta\tilde{G}_M$ , and  $\tilde{G}_E = G_E + \delta\tilde{G}_E$ , where  $G_M$  and  $G_E$  are the usual proton magnetic and electric form factors, which are functions of  $Q^2$  only and are defined from matrix elements of the electromagnetic current. The amplitudes  $\tilde{F}_3 = \delta\tilde{F}_3$ ,  $\delta\tilde{G}_M$ , and  $\delta\tilde{G}_E$ , originate from processes involving the exchange of at least two photons, and are of order  $e^2$  (relative to the factor  $e^2$  in Eq. (9)).

The unpolarized cross section is

$$\frac{d\sigma}{d\Omega_{Lab}} = \frac{\tau\sigma_R}{\epsilon(1 + \tau)} \frac{d\sigma_{NS}}{d\Omega_{Lab}}, \quad (12)$$

where the “no structure” cross section is

$$\frac{d\sigma_{NS}}{d\Omega_{Lab}} = \frac{4\alpha^2 \cos^2(\theta/2)}{Q^4} \frac{E'^3}{E}, \quad (13)$$

and  $E$  and  $E'$  are the incoming and outgoing electron Lab energies. Other quantities are defined after Eq. (1). The reduced cross section including the two-photon exchange correction becomes [19]

$$\sigma_R = G_M^2 + \frac{\epsilon}{\tau} G_E^2 + 2 G_M \mathcal{R} \left( \delta\tilde{G}_M + \epsilon \frac{\nu}{M^2} \tilde{F}_3 \right) + 2 \frac{\epsilon}{\tau} G_E \mathcal{R} \left( \delta\tilde{G}_E + \frac{\nu}{M^2} \tilde{F}_3 \right) + \mathcal{O}(e^4), \quad (14)$$

where  $\mathcal{R}$  stands for the real part.

The general expressions for the double polarization observables, including two-photon exchange, are [19]:

$$\begin{aligned} P_s &= A_s = \\ &= -\sqrt{\frac{2\epsilon(1 - \epsilon)}{\tau}} \frac{(2h_e)}{\sigma_R} \left\{ G_E G_M + G_E \mathcal{R}(\delta\tilde{G}_M) + G_M \mathcal{R} \left( \delta\tilde{G}_E + \frac{\nu}{M^2} \tilde{F}_3 \right) + \mathcal{O}(e^4) \right\}, \\ P_l &= -A_l = \sqrt{1 - \epsilon^2} \frac{(2h_e)}{\sigma_R} \left\{ G_M^2 + 2 G_M \mathcal{R} \left( \delta\tilde{G}_M + \frac{\epsilon}{1 + \epsilon} \frac{\nu}{M^2} \tilde{F}_3 \right) + \mathcal{O}(e^4) \right\}, \end{aligned} \quad (15)$$

where  $h_e = \pm 1/2$  is the helicity of the electron and we assumed  $m_e = 0$ . The polarizations are related to the analyzing powers  $A_s$  or  $A_l$ , by time-reversal invariance. That the polarization  $P_l$  is unity in the backward direction,  $\epsilon = 0$ , follows generally from lepton helicity conservation and angular momentum conservation.

## 2.3 Two-photon exchange at the quark level

In order to estimate the two-photon exchange contribution to  $\tilde{G}_M$ ,  $\tilde{F}_2$  and  $\tilde{F}_3$  at large momentum transfers, we will consider a partonic calculation illustrated in Fig. 2. To begin, we calculate the subprocess on a quark, denoted by the scattering amplitude  $H$

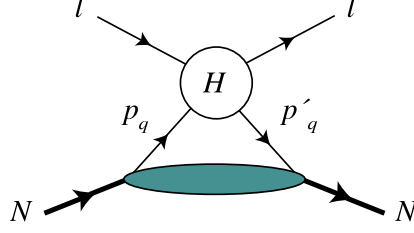


Figure 2: Handbag approximation for the elastic lepton-nucleon scattering at large momentum transfers. In the partonic scattering process (indicated by  $H$ ), the lepton scatters from quarks in the nucleon, with momenta  $p_q$  and  $p'_q$ . The lower blob represents the GPDs of the nucleon.

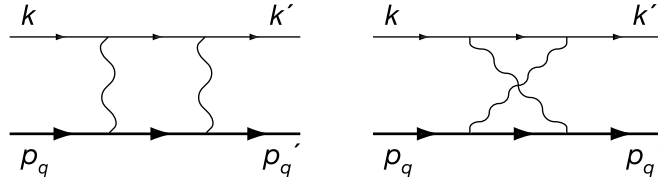


Figure 3: Direct and crossed box diagrams to describe the two-photon exchange contribution to the lepton-quark scattering process, corresponding with the blob denoted by  $H$  in Fig. 2.

in Fig. 2. Subsequently, we shall embed the quarks in the proton as described through the nucleon's generalized parton distributions (GPDs).

Elastic lepton-quark scattering,

$$l(k) + q(p_q) \rightarrow l(k') + q(p'_q) , \quad (16)$$

is described by two independent kinematical invariants,  $\hat{s} \equiv (k + p_q)^2$  and  $Q^2 = -t = -(k - k')^2$ . We also introduce the crossing variable  $\hat{u} \equiv (k - p'_q)^2$ , which satisfies  $\hat{s} + \hat{u} = Q^2$ . The  $T$ -matrix for the two-photon part of the electron-quark scattering can be written as

$$H_{h,\lambda} = \frac{(e e_q)^2}{Q^2} \bar{u}(k', h) \gamma_\mu u(k, h) \cdot \bar{u}(p'_q, \lambda) \left( \tilde{f}_1 \gamma^\mu + \tilde{f}_3 \gamma \cdot K P_q^\mu \right) u(p_q, \lambda), \quad (17)$$

with  $P_q \equiv (p_q + p'_q)/2$ , where  $e_q$  is the fractional quark charge (for a flavor  $q$ ), and where  $u(p_q, \lambda)$  and  $u(p'_q, \lambda)$  are the quark spinors with quark helicity  $\lambda = \pm 1/2$ , which is conserved in the scattering process for massless quarks. Quark helicity conservation leads to the absence of any analog of  $\tilde{F}_2$  in the general expansion of Eq. (9).

The partonic scattering helicity amplitudes  $H_{h,\lambda}$  of Eq. (17) at order  $O(e^4)$  are given by the two-photon exchange direct and crossed box diagrams of Fig. 3. The two-photon exchange contribution to the elastic electron-scattering off spin 1/2 Dirac particles was first calculated in Ref. [42], which was verified explicitly for the work reported in [36, 37]. The amplitude  $\tilde{f}_1$ , but not  $\tilde{f}_3$ , has an infrared (IR) divergence, which we isolate into a soft part, *i.e.*,  $\tilde{f}_1 = \tilde{f}_1^{soft} + \tilde{f}_1^{hard}$ . The soft part corresponds with the situation where one of the photons in Fig. 3 carries zero four-momentum, and is obtained by replacing the other photon's four-momentum by  $q$  in both numerator and denominator of the loop

integral [43]. This yields,

$$\mathcal{R}(\tilde{f}_1^{soft}) = \frac{e^2}{4\pi^2} \left\{ \ln \left( \frac{\lambda^2}{\sqrt{-\hat{s}\hat{u}}} \right) \ln \left| \frac{\hat{s}}{\hat{u}} \right| + \frac{\pi^2}{2} \right\}, \quad (18)$$

where  $\lambda$  is an infinitesimal photon mass controlling the IR divergence. The remaining  $\tilde{f}_i$  can be found in [36, 37].

The full electron-quark elastic cross section, using Eq. (14), is

$$d\sigma = d\sigma_{1\gamma} \left[ 1 + 2\mathcal{R}(\tilde{f}_1)_{2\gamma} + \varepsilon \frac{\hat{s} - \hat{u}}{4} 2\mathcal{R}(\tilde{f}_3)_{2\gamma} \right] \equiv d\sigma_{1\gamma} (1 + \delta_{2\gamma}), \quad (19)$$

where  $d\sigma_{1\gamma}$  is the cross section in the one-photon exchange approximation,  $\varepsilon = -2\hat{s}\hat{u}/(\hat{s}^2 + \hat{u}^2)$  in the massless limit, and one can easily obtain  $\delta_{2\gamma}$  from the  $\tilde{f}_i$ .

## 2.4 Calculation using generalized parton distributions

Having calculated the partonic subprocess, we next discuss how to embed the quarks in the nucleon. We begin by discussing the soft contributions. The handbag diagrams discussed so far have both photons coupled to the same quark. There are also contributions from processes where the photons interact with different quarks. One can show that the IR contributions from these processes, which are proportional to the products of the charges of the interacting quarks, added to the soft contributions from the handbag diagrams give the same result as the soft contributions calculated with just a nucleon intermediate state [44]. Thus the low energy theorem for Compton scattering is satisfied. In the handbag approximation, the hard parts which appear when the photons couple to different quarks, the so-called cat's ears diagrams, are neglected.

For the real parts, the IR divergence arising from the direct and crossed box diagrams, at the nucleon level, is cancelled when adding the bremsstrahlung contribution from the interference of diagrams where a soft photon is emitted from the electron and from the proton. This provides a radiative correction term from the soft part of the boxes plus electron-proton bremsstrahlung which added to the lowest order term may be written as

$$\sigma_{soft} = \sigma_{1\gamma} (1 + \delta_{2\gamma, soft} + \delta_{brems}^{ep}), \quad (20)$$

where  $\sigma_{1\gamma}$  is the one-photon exchange cross section. In Eq. (20), the soft-photon contribution due to the nucleon box diagram is given by

$$\begin{aligned} \delta_{2\gamma, soft} = \frac{e^2}{2\pi^2} & \left\{ \ln \left( \frac{\lambda^2}{\sqrt{(s-M^2)|u-M^2|}} \right) \ln \left| \frac{s-M^2}{u-M^2} \right| \right. \\ & \left. - L \left( \frac{s-M^2}{s} \right) - \frac{1}{2} \ln^2 \left( \frac{s-M^2}{s} \right) + \mathcal{R} \left[ L \left( \frac{u-M^2}{u} \right) \right] + \frac{1}{2} \ln^2 \left( \frac{u-M^2}{u} \right) + \frac{\pi^2}{2} \right\}, \end{aligned} \quad (21)$$

where  $L$  is the Spence function defined by

$$L(z) = - \int_0^z dt \frac{\ln(1-t)}{t}. \quad (22)$$

The bremsstrahlung contribution where a soft photon is emitted from an electron and proton line (*i.e.*, by cutting one of the (soft) photon lines in Fig. 3) was calculated in

Ref. [45], which we verified explicitly, and is for the case that the outgoing electron is detected,

$$\begin{aligned} \delta_{brems}^{ep} = & \frac{e^2}{2\pi^2} \left\{ \ln \left( \frac{4 (\Delta E)^2 (s - M^2)^2}{\lambda^2 y (u - M^2)^2} \right) \ln \left( \frac{s - M^2}{M^2 - u} \right) \right. \\ & \left. + L \left( 1 - \frac{1}{y} \frac{s - M^2}{M^2 - u} \right) - L \left( 1 - \frac{1}{y} \frac{M^2 - u}{s - M^2} \right) \right\}, \end{aligned} \quad (23)$$

where  $\Delta E \equiv E_e'^{el} - E_e'$  is the difference of the measured outgoing electron *lab* energy ( $E_e'$ ) from its elastic value ( $E_e'^{el}$ ), and  $y \equiv (\sqrt{\tau} + \sqrt{1 + \tau})^2$ . One indeed verifies that the sum of Eqs. (21,23) is IR finite. When comparing with elastic *ep* cross section data, which are usually radiatively corrected using the procedure of Mo and Tsai, Ref. [13], we have to consider only the difference of our  $\delta_{2\gamma, soft} + \delta_{brems}^{ep}$  relative to the  $\mathcal{O}(Z^2)$  part, in their notation, of the radiative correction in [13]. Except for the  $\pi^2/2$  term in Eq. (21), this difference was found to be below  $10^{-3}$  for all kinematics considered in Fig. 4.

After some algebra, one obtains the hard  $2\gamma$  exchange contributions to  $\delta\tilde{G}_M$ ,  $\delta\tilde{G}_E$ , and  $\tilde{F}_3$  as,

$$\delta\tilde{G}_M^{hard} = C, \quad (24)$$

$$\delta\tilde{G}_E^{hard} = - \left( \frac{1 + \varepsilon}{2\varepsilon} \right) (A - C) + \sqrt{\frac{1 + \varepsilon}{2\varepsilon}} B, \quad (25)$$

$$\tilde{F}_3 = \frac{M^2}{\nu} \left( \frac{1 + \varepsilon}{2\varepsilon} \right) (A - C), \quad (26)$$

with

$$\begin{aligned} A &\equiv \int_{-1}^1 \frac{dx}{x} \frac{[(\hat{s} - \hat{u}) \tilde{f}_1^{hard} - \hat{s} \hat{u} \tilde{f}_3]}{(s - u)} \sum_q e_q^2 (H^q + E^q), \\ B &\equiv \int_{-1}^1 \frac{dx}{x} \frac{[(\hat{s} - \hat{u}) \tilde{f}_1^{hard} - \hat{s} \hat{u} \tilde{f}_3]}{(s - u)} \sum_q e_q^2 (H^q - \tau E^q), \\ C &\equiv \int_{-1}^1 \frac{dx}{x} \tilde{f}_1^{hard} \text{sgm}(x) \sum_q e_q^2 \tilde{H}^q. \end{aligned} \quad (27)$$

The functions  $H^q$ ,  $E^q$ , and  $\tilde{H}^q$  are the generalized parton distributions, which describe removing a quark of a certain momentum from a hadron, and replacing it with a quark of another momentum (or, even, in a more general case, with one of a different flavor). One can see from Fig. 2 that these are just what we need to knit the amplitudes for electron-quark scattering into an amplitude involving the proton. There is a fourth GPD,  $\tilde{E}^q$ , that does not enter the two-photon exchange expressions. The GPDs can be measured in deeply virtual or wide-angle Compton scattering, and have been reviewed in [21, 22, 23, 24] and elsewhere. The GPD models we use here are detailed in [37, 46]; so also [47].

From the integrals  $A$ ,  $B$ , and  $C$ , and the usual form factors, we can directly construct the observables. The cross section is

$$\sigma_R = \sigma_{R, soft} + \sigma_{R, hard}, \quad (28)$$

where

$$\sigma_{R,hard} = (1 + \varepsilon) G_M \mathcal{R}(A) + \sqrt{2\varepsilon(1 + \varepsilon)} \frac{1}{\tau} G_E \mathcal{R}(B) + (1 - \varepsilon) G_M \mathcal{R}(C) . \quad (29)$$

From Eqs. (20) to (23) and the discussion surrounding them, we learned that to a good approximation the result for the soft part can be written as

$$\sigma_{R,soft} = \sigma_{R,1\gamma} \left( 1 + \pi\alpha + \delta^{MT} \right) , \quad (30)$$

where  $\delta^{MT}$  is the correction given in Ref. [13]. Since the data is very commonly corrected using [13], let us define  $\sigma_R^{MT\ corr} \equiv \sigma_R / (1 + \delta^{MT})$ . Then an accurate relationship between the data with Mo-Tsai corrections already included and the form factors is

$$\sigma_R^{MT\ corr} = \left( G_M^2 + \frac{\varepsilon}{\tau} G_E^2 \right) (1 + \pi\alpha) + \sigma_{R,hard} , \quad (31)$$

where the left hand side is what experimenters often quote as radiatively corrected data. Since the Mo-Tsai corrections are so commonly made in experimental papers before reporting the data, the “*MT corr*” superscript will be understood rather than explicit when we show cross section plots below. The extra terms on the right-hand-side come from new two-photon exchange corrections. The reader may marginally improve the expression by including with the  $(1 + \pi\alpha)$  factor the circa 0.1% difference between our actual soft results and those of [13]. Finally, before discussing polarization, the fact that a  $\pi^2/2$  term, or  $(\pi\alpha)$  term after multiplying in the overall factors, sits in the soft corrections has to do with the specific criterion we used, that of Ref. [43], to separate the soft from hard parts. The term cannot be eliminated; with a different criterion, however, that term can move into the hard part.

The double polarization observables of Eqs. (15) are given by

$$P_s = -\sqrt{\frac{2\varepsilon(1 - \varepsilon)}{\tau}} \frac{1}{\sigma_R} \left\{ G_E G_M + G_E \mathcal{R}(C) + G_M \sqrt{\frac{1 + \varepsilon}{2\varepsilon}} \mathcal{R}(B) + \mathcal{O}(e^4) \right\} , \quad (32)$$

$$P_l = \sqrt{1 - \varepsilon^2} \frac{1}{\sigma_R} \left\{ G_M^2 + G_M \mathcal{R}(A + C) + \mathcal{O}(e^4) \right\} . \quad (33)$$

## 2.5 Results

### 2.5.1 Cross section

Figure 4 shows the reduced differential cross section for electron-proton scattering  $\sigma_R$ , for two values of  $Q^2$ . There are three items on each graph. One is the data. The next is the straight line, which is the result of the 1- $\gamma$  exchange calculation using  $G_E/G_M$  taken from the polarization data [6], with a reasonable and commonly used choice for  $G_M$  [48]. The slope is too flat to fit the data, reflecting the conflict between the polarization measurements and the Rosenbluth measurements with the hard 2- $\gamma$  corrections. Third are the slightly curved lines, showing the results of the 2- $\gamma$  corrections while still using the  $G_E/G_M$  ratio from the polarization data. Results are shown for two different model GPDs, described in [36, 37, 46]; they do not greatly differ. (The renormalization of  $G_M$  that we have allowed does not affect the slope.) One sees that the hard 2- $\gamma$  corrections steepen the average slope and improve the agreement with the data. It is also important

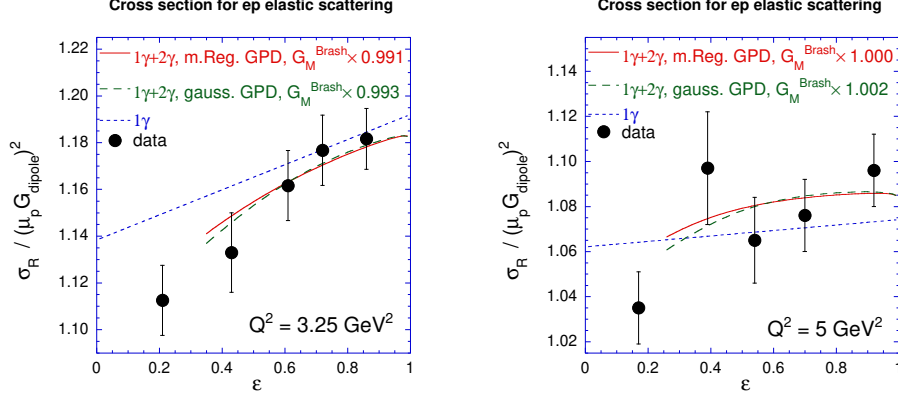


Figure 4: Rosenbluth plots for elastic  $ep$  scattering:  $\sigma_R$  divided by  $(\mu_p G_D)^2$ , with  $G_D = (1 + Q^2/0.71)^{-2}$ . Dotted curves: Born approximation using  $G_E/G_M$  from polarization data [5, 6]. Solid curves: full calculation using the modified Regge GPD, for the kinematical range  $-u > M^2$ . Dashed curves: same as solid curves but using the gaussian GPD. The data are from Ref. [8]; the Figure and calculation are from Ref. [37].

to note the non-linearity in the Rosenbluth plot, which can be checked with a more precise experiment.

Fig. 5 presents the  $2\gamma$  results in a different way. The plot shows the extracted  $G_E/G_M$  vs.  $Q^2$ . One set of data points, falling linearly with  $Q^2$ , is from the polarization experiments. Another set of data points, roughly constant in  $Q^2$  and plotted with inverted triangles, is from Rosenbluth data analyzed using only the Mo-Tsai [13] radiative corrections. The solid squares show the best fit  $G_E/G_M$  from the Ref. [8] data when analyzed including the hard  $2\gamma$  corrections. One sees that for  $Q^2$  in the 2–3  $\text{GeV}^2$  range, the  $G_E/G_M$  extracted using the Rosenbluth method including the  $2\gamma$  corrections agree well with the polarization transfer results; At higher  $Q^2$ , there is at least partial reconciliation between the two methods.

There is one more point on Fig. 5, which shows the result of also including some hard bremsstrahlung corrections, which will be discussed below.

### 2.5.2 Polarization transfers

The  $2\gamma$  corrections do not impact the polarizations measurements as strongly as the Rosenbluth measurements. The left panel of Fig. 6 shows the correction to the  $P_s/P_l$  ratio from the hard  $2\gamma$  exchange. Most of the effect is on  $P_s$ , shown separately in the right panel of the same Figure; the effect on  $P_l$  is too small to show on Figures like these. The present polarization experiments have  $\varepsilon \approx 0.7$ . The  $2\gamma$  corrections induce an  $\varepsilon$ -dependence that could be seen in a precise experiment [49].

### 2.5.3 Positron-proton vs. electron-proton

Positron-proton and electron-proton scattering have the opposite sign for the two-photon corrections relative to the one-photon terms. Hence one expects  $e^+p$  and  $e^-p$  elastic scattering to differ by a few percent. Figure 7 shows our results for three different  $Q^2$  values. These curves are obtained by adding our two-photon box calculation, minus the corresponding part of the soft only calculation in [13], to the one-photon calculations;

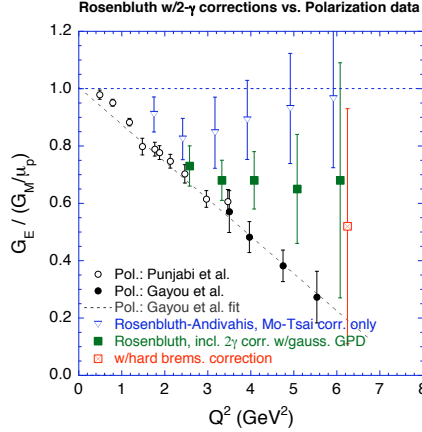


Figure 5: Determinations of the proton  $G_E/G_M$  ratio. The polarization data is from Gayou *et al.* [6] and Punjabi *et al.* [7], and the Rosenbluth data is from Andivahis *et al.* [8], which include only the well-known Mo-Tsai corrections. Our Rosenbluth  $G_E/G_M$  include the two-photon corrections, and for one point also a hard bremsstrahlung correction, still using Andivahis *et al.* data. Some of our points for the Rosenbluth results are slightly offset horizontally for clarity.

hence, they are meant to be compared to data where the corrections given in [13] have already been made. Each curve is based on the gaussian GPD and is cut off at low  $\varepsilon$  when  $-u = M^2$ . Early data from SLAC are available [11]; more precise data are anticipated from JLab [50]. (Ref. [11] used the Meister-Yennie [14] soft corrections rather than those of Mo and Tsai. We have checked that for these kinematics the difference between them is smaller than 0.1%, which is negligible compared to the size of the error bars.)

#### 2.5.4 Results from single-baryon intermediate states

We have focused on a partonic view of the two-photon physics. The results when viewing the hadronic intermediate state as a proton, or a proton plus a set of resonances, are similar [31, 32, 33, 34, 35]. The effect, in a calculation with just a proton intermediate state, of the extra 2- $\gamma$  corrections upon extracting  $G_E/G_M$  from a Rosenbluth experiment is shown in Fig. 8. Further, corrections to the polarization experiments are just a few percent, in the same direction as found in the partonic evaluation, with nearly all the effect coming upon  $P_s$  and not on  $P_l$  [32].

## 2.6 Remarks on related topics

There has been a suggestion that hard bremsstrahlung may cause the difference between the Rosenbluth and polarization results [51]. Bremsstrahlung means a process where a real photon is emitted. If the photon energy is sufficiently low, the experimenters will fail to see it and will count the reaction as elastic. Usual bremsstrahlung calculations are for soft bremsstrahlung, where the emitted photon energy is kept only to linear order in denominators and entirely omitted in numerators. Soft bremsstrahlung multiplies all amplitudes by the same factor and does not, for a relevant example, change the slope on a Rosenbluth plot. If one makes no approximations in the photon energy, there can be different effects on different spin amplitudes. Thus the claim is that emitted



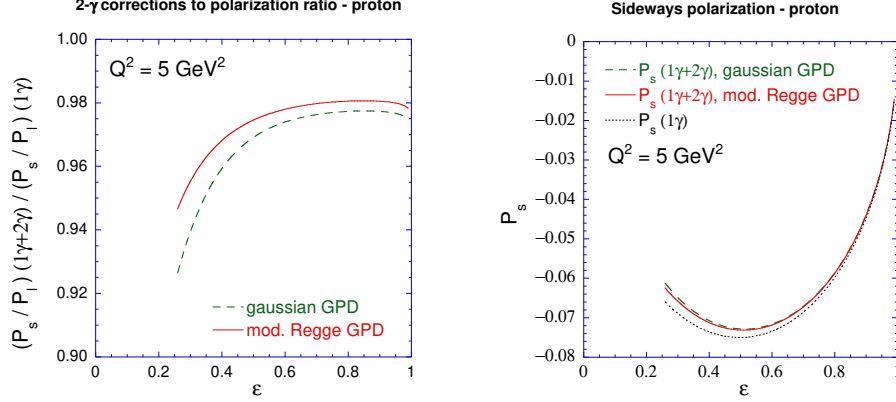


Figure 6: Polarization  $P_s/P_l$  and  $P_s$  compared to the  $1\gamma$  exchange results for  $ep$  scattering at  $Q^2 = 5 \text{ GeV}^2$ . The solid and dashed curves show the  $2\gamma$  exchange correction using the GPD calculation, for the kinematical range where both  $s, -u > M^2$ . The dotted curves on the right shows the Born approximation ( $1\gamma$  exchange) result.

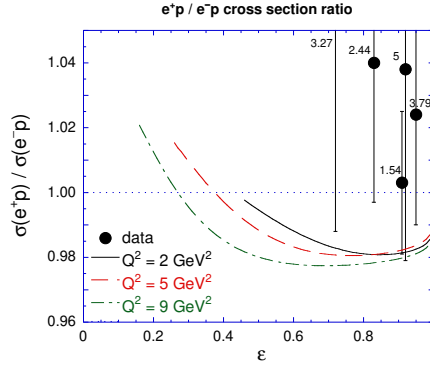


Figure 7: Ratio of  $e^+/e^-$  elastic cross sections on the proton. The GPD calculations of the  $2\gamma$  correction are for  $Q^2$  of 2, 5, and 9  $\text{GeV}^2$ , for the kinematical range with  $-u$  above  $M^2$ . Also shown are all known data, from [11], with  $Q^2$  above 1.5  $\text{GeV}^2$  (the missing central value is at 1.111). The numbers near the data give  $Q^2$  for that point in  $\text{GeV}^2$ .

photons that are energetic enough to affect the spin structure of the calculation but still small enough to escape detection, give rise to the difference between the two methods of measuring  $G_E/G_M$ . A contrasting numerical claim is that hard bremsstrahlung effects are noticeable and helpful in reconciling the Rosenbluth and polarization experiments, but are not decisive. Along these lines is a result for hard bremsstrahlung at  $Q^2 = 6 \text{ GeV}^2$  from Afanasev [52], which has been added to the  $2\gamma$  results and included in Fig. 5.

These contrasting claims clearly need adjudication, but an independent reexamination is not available as of this writing.

Electron, or muon, scattering off deuterons or larger nuclei has not been within the scope of the present review. Larger nuclei have a factor  $Z$  advantage in the relative size of the  $2\gamma$  and  $1\gamma$  effects, although breakup effects vitiate this advantage for elastic scattering except at low energy. One can examine some of the work seeking evidence of  $2\gamma$  effects in larger nuclei in [53, 54, 55, 56, 57].

Two-photon exchange effects also affect parity-violating  $e-p$  elastic scattering via their

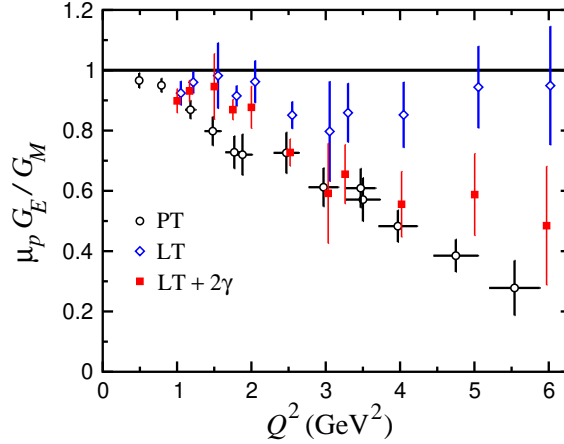


Figure 8: Extracting  $G_E/G_M$  with  $2\gamma$  corrections calculated using a single proton as the hadronic intermediate state. “PT” is  $G_E/G_M$  obtained from the polarization transfer experiments; “LT” is  $G_E/G_M$  obtained from a Rosenbluth experiment using only the Mo-Tsai radiative corrections, and “LT+ $2\gamma$ ” includes the extra  $2\gamma$  corrections done this way. This figure is based on a figure in Ref. [32], and we thank the authors for providing it.

interference with the lowest order  $Z$ -exchange diagram. Ref. [59] pointed this out, and found that the  $2\gamma$  exchange also led to extra terms with different  $\tau$  and  $\varepsilon$  dependences than those known from analyses using only Born diagrams. The calculated size of the effects, using the partonic model at  $Q^2$  of several  $\text{GeV}^2$ , was of  $\mathcal{O}(1\%)$ . This is below present experimental uncertainties, but parity-violating experiments with  $\mathcal{O}((1/2)\%)$  uncertainties are planned.

Arrington and Sick [58], considering the effects that the most recent and precise low- $Q^2$  determinations of  $G_E$  and  $G_M$  would have upon parity-violating  $e$ - $p$  elastic scattering, and included the two photon correction terms that were pointed out in [59]. The actual two-photon calculations at their  $Q^2$  were done using single hadron intermediate states [60].

### 3 Polarizability corrections to hydrogen hyperfine splitting

#### 3.1 Two-photon exchange and atomic structure

We begin with some explanation of how this piece of atomic physics fits properly into a review of two-photon physics. Hydrogen hyperfine splitting (hfs) in the ground state is known to 13 significant figures in frequency units [61],

$$E_{\text{hfs}}(e^-p) = 1\,420.405\,751\,766\,7(9)\text{ MHz}. \quad (34)$$

This accuracy is remarkable to theorists, who are currently hopeful of obtaining a calculation accurate to a part per million (ppm). To reach this goal, some improvement is needed, and the current best calculations are a few ppm away from the data.

The main uncertainty in calculating the hfs in hydrogen comes from the hadronic, or proton structure, corrections. The generic process that contributes is two-photon exchange, shown in Fig. 9a, which involves the proton structure because each of the exchanged photons could individually be quite energetic.

One-photon exchange, Fig. 9b, does not involve proton structure, at the accuracy needed for the present purpose. The characteristic momentum of the electron in a hydrogen atom is of  $\mathcal{O}(\alpha m_e)$ , which is very low on a nuclear physics scale. Hence the  $q^2$  of an exchanged single photon is very low, and the variation of the proton form factor from its  $q^2 = 0$  value is minimal. One can show that keeping the electron momentum gives corrections of  $\mathcal{O}(\alpha m_e/M)$  smaller than what comes from two-photon exchange. Hence one sets the momenta of the electrons to zero. (For information, in the one-photon exchange hfs calculation there comes a  $q^2$  factor in the numerator which cancels the  $1/q^2$  from the photon propagator; then the neglect of the electron momenta is safe.)

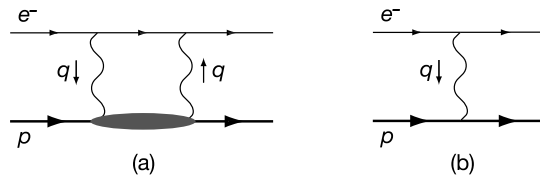


Figure 9: (a) Generic two-photon exchange diagram, giving proton-structure corrections to hyperfine splitting. (b) One-photon exchange.

#### 3.2 Hyperfine splitting calculations

The calculated hyperfine splitting in hydrogen is [61, 62, 63],

$$E_{\text{hfs}}(e^-p) = (1 + \Delta_{\text{QED}} + \Delta_{\text{weak}}^p + \Delta_{\text{str}}) E_F^p; \quad (35)$$

the two-photon exchange lies in the structure dependent term  $\Delta_{\text{str}}$ . The Fermi energy is

$$E_F^p = \frac{8\alpha^3 m_r^3}{3\pi} \mu_B \mu_p = \frac{16\alpha^2}{3} \frac{\mu_p}{\mu_B} \frac{R_\infty}{(1 + m_e/M)^3}, \quad (36)$$

where  $m_r = m_e M / (M + m_e)$  is the reduced mass. By convention, in  $E_F^p$  one uses the actual magnetic moment for the proton and the Bohr magneton for the electron (note that  $\mu_B$  can be used to replace the electron mass), and  $R_\infty$  is the Rydberg constant in frequency units. The second form allows optimal accuracy in evaluating  $E_F^p$ . The least accurately known quantity is the ratio  $\mu_p / \mu_B$ , which is known to 8 figures. Hence to the ppm level,  $E_F^p$  is known more than sufficiently well. The QED [26, 27] and weak interaction corrections [64] are well known and will not be discussed, except to mention that the QED corrections could be obtained, for the present purposes, without calculation. They are the same as for muonium, so it is possible to obtain them to an accuracy more than adequate for the present purpose using muonium hfs data and a judicious scaling [65, 66].

The structure dependent corrections are, in a standard treatment, divided into Zemach, recoil, and polarizability corrections,

$$\Delta_{\text{str}} = \Delta_Z + \Delta_R^p + \Delta_{\text{pol}}. \quad (37)$$

The first two terms arise when the blob in Fig. 9a is just a proton, as in Fig. 10, and they are together called the elastic corrections. The electron-photon vertex is well known, and the proton-photon vertex is given by [67, 68]

$$\Gamma_\mu = \gamma_\mu F_1(Q^2) + \frac{i}{2M} \sigma_{\mu\nu} q^\nu F_2(Q^2) \quad (38)$$

(for the photon with incoming momentum  $q$ ) if the intermediate proton is on-shell. Of course, it is generally not. However, one can show that the imaginary part of the diagram does come only from kinematics where the intermediate electron and proton are on-shell. Hence, one can correctly use the above vertex to calculate the imaginary part of the diagrams, and then obtain the whole of the diagram using a dispersion relation.

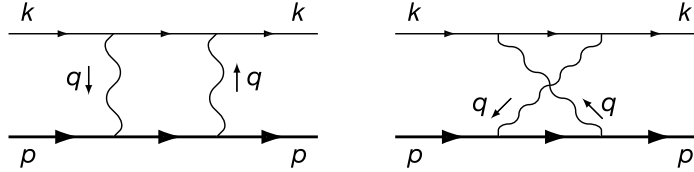


Figure 10: Two-photon exchange diagrams for the “elastic” proton-structure corrections to hyperfine splitting.

In the nonrelativistic limit, the recoil terms are zero and the Zemach term is not. (The nonrelativistic limit is  $M \rightarrow \infty$ , with  $m_e$  and the proton size held fixed. Proton size information is embedded in the form factors  $F_1$  and  $F_2$ .) The Zemach term [69] was calculated long ago and in modern form is,

$$\Delta_Z = \frac{8\alpha m_r}{\pi} \int_0^\infty \frac{dQ}{Q^2} \left[ G_E(Q^2) \frac{G_M(Q^2)}{1 + \kappa_p} - 1 \right] = -2\alpha m_r r_Z, \quad (39)$$

the last equality defining the Zemach radius  $r_Z$ . The charge and magnetic form factors are linear combinations of  $F_1$  and  $F_2$ ,

$$\begin{aligned} G_M &= F_1 + F_2, \\ G_E &= F_1 - \frac{Q^2}{4M^2} F_2. \end{aligned} \quad (40)$$

The recoil corrections won't be explicitly displayed in this paper because they are somewhat long (although not awful; see [67, 68]). An important point is that they do depend on the form factors and hence upon the proton structure. However, their numerical value is fairly steady by present standards of accuracy when they are evaluated using different up-to-date analytic form factors based on fits to the scattering data.

One gets the polarizability corrections by summing all contributions where the intermediate hadronic state, the blob in Fig. 9a, is not a single photon. Paralleling the elastic case, one can show that the imaginary part of this diagram comes only from configurations where the intermediate electron plus hadronic state is kinematically on-shell, *i.e.*, physically realizable. Hence one can calculate the imaginary part of the box diagram if one has data on inelastic electron-proton scattering. Then, further paralleling the elastic case, one obtains the full box diagram via a dispersion relation.

To see some detail, the lower half of Fig. 9a is the same as forward Compton scattering of off-shell photons from protons, which is given in terms of the matrix element

$$T_{\mu\nu}(q, p, S) = \frac{i}{2\pi M} \int d^4\xi \, e^{iq\cdot\xi} \langle pS | T \{ j_\mu(\xi), j_\nu(0) \} | pS \rangle, \quad (41)$$

where  $j_\mu$  is the electromagnetic current and the states are proton states of momentum  $p$  and spin 4-vector  $S$ . The spin dependence is in the antisymmetric part

$$T_{\mu\nu}^A = \frac{i}{M\nu} \epsilon_{\mu\nu\alpha\beta} q^\alpha \left[ \left( H_1(\nu, q^2) + H_2(\nu, q^2) \right) S^\beta - H_2(\nu, q^2) \frac{S \cdot q \, p^\beta}{p \cdot q} \right]. \quad (42)$$

The two structure functions  $H_1$  and  $H_2$  depend on  $q^2$  and on the lab frame photon energy  $\nu$ , defined by  $M\nu = p \cdot q$ .

The optical theorem that relates the imaginary part of the forward Compton amplitude to the inelastic scattering cross section for off-shell photons on protons. The relations precisely are

$$\text{Im } H_1(\nu, q^2) = \frac{1}{\nu} g_1(\nu, q^2) \quad \text{and} \quad \text{Im } H_2(\nu, q^2) = \frac{M}{\nu^2} g_2(\nu, q^2), \quad (43)$$

where  $g_1$  and  $g_2$  are functions appearing in the cross section and are measured [70, 71, 72, 73, 74] at SLAC, HERMES, JLab, and elsewhere.

Using the Compton amplitude to evaluate the inelastic part of the two-photon loops leads to

$$\begin{aligned} \Delta_{\text{pol}} &= \frac{E_{2\gamma}}{E_F} \Big|_{\text{inel}} = \frac{2\alpha m_e}{(1 + \kappa_p)\pi^3 M} \\ &\times \int \frac{d^4Q}{(Q^4 + 4m_e^2 Q_0^2)Q^2} \left\{ (2Q^2 + Q_0^2) H_1^{\text{inel}}(iQ_0, -Q^2) - 3Q^2 Q_0^2 H_2^{\text{inel}}(iQ_0, -Q^2) \right\}, \end{aligned} \quad (44)$$

where we have Wick rotated the integral so that  $Q_0 = -i\nu$ ,  $\vec{Q} = \vec{q}$ , and  $Q^2 \equiv Q_0^2 + \vec{Q}^2$ . The dispersion relations which gives  $H_1$  is, assuming no subtraction,

$$H_1^{\text{inel}}(\nu_1, q^2) = \frac{1}{\pi} \int_{\nu_{\text{th}}}^{\infty} d\nu \frac{\text{Im } H_1(\nu, q^2)}{\nu^2 - \nu_1^2}, \quad (45)$$

where the integral is only over the inelastic region, and a similar relation holds for  $H_2$ . The no-subtraction assumption will be discussed later.

Integrating what can be integrated, and neglecting  $m_e$  inside the integral, yields the expression [75, 76, 77, 78, 79, 80]

$$\Delta_{\text{pol}} = \frac{\alpha m_e}{2(1 + \kappa_p)\pi M}(\Delta_1 + \Delta_2), \quad (46)$$

where, with  $\tau = \nu^2/Q^2$ ,

$$\Delta_1 = \frac{9}{4} \int_0^\infty \frac{dQ^2}{Q^2} \left\{ F_2^2(Q^2) + 4M \int_{\nu_{th}}^\infty \frac{d\nu}{\nu^2} \beta(\tau) g_1(\nu, Q^2) \right\}, \quad (47)$$

$$\Delta_2 = -12M \int_0^\infty \frac{dQ^2}{Q^2} \int_{\nu_{th}}^\infty \frac{d\nu}{\nu^2} \beta_2(\tau) g_2(\nu, Q^2).$$

The auxiliary functions are

$$\begin{aligned} \beta(\tau) &= \frac{4}{9} \left[ -3\tau + 2\tau^2 + 2(2 - \tau)\sqrt{\tau(\tau + 1)} \right], \\ \beta_2(\tau) &= 1 + 2\tau - 2\sqrt{\tau(\tau + 1)}. \end{aligned} \quad (48)$$

The integral for  $\Delta_1$  actually requires further comment. Only the second terms comes from the procedure just outlined; it was historically thought convenient to add the first term, and then subtract the same term from the the recoil corrections. This stratagem allows the electron mass to be taken to zero in  $\Delta_1$ . The individual terms in  $\Delta_1$  diverge (they would not had the electron mass been kept), but the whole is finite because of the Gerasimov-Drell-Hearn (GDH) [81, 82] sum rule,

$$4M \int_{\nu_{th}}^\infty \frac{d\nu}{\nu^2} g_1(\nu, 0) = -\kappa_p^2, \quad (49)$$

coupled with the observation that the auxiliary function  $\beta(\tau)$  becomes unity as we approach the real photon point.

### 3.3 Numerics, especially for $\Delta_{\text{pol}}$

We start this numerical section with a brief discussion of the polarizability corrections. They have some history. Considerations of  $\Delta_{\text{pol}}$  were begun by Iddings in 1965 [75], improved by Drell and Sullivan in 1966[76], and given in present notation by de Rafael in 1971 [77]. But no sufficient spin-dependent data existed, so it was several decades before the formula could be evaluated to a result incompatible with zero. In 2002, Faustov and Martynenko became the first to use  $g_{1,2}$  data to obtain results inconsistent with zero [79]. They got

$$\Delta_{\text{pol}}(\text{F\&M 2002}) = (1.4 \pm 0.6) \text{ ppm} \quad (50)$$

However, only SLAC data was available. None of the SLAC data had  $Q^2$  below 0.30  $\text{GeV}^2$ ;  $\Delta_1$  and  $\Delta_2$  are sensitive to the behavior of the structure functions at low  $Q^2$ . Also in 2002 there appeared analytic expressions for  $g_{1,2}$  fit to data by Simula, Osipenko, Ricco, and Taiuti [83], which included JLab as well as SLAC data. Simula *et al.* did not integrate their results to obtain  $\Delta_{\text{pol}}$ , but had they done so, they would have obtained  $\Delta_{\text{pol}} = (0.4 \pm 0.6) \text{ ppm}$  [80].

More recently Faustov and Martynenko, joined by Gorbacheva, [84] have reanalyzed their result for  $\Delta_{\text{pol}}$ , and obtained a somewhat larger value,

$$\Delta_{\text{pol}}(\text{FGM 2006}) = (2.2 \pm 0.8) \text{ ppm} . \quad (51)$$

The data underlying this result, however, still does not include the lower  $Q^2$  data from JLab that will be noted immediately below.

Data for  $g_1(\nu, q^2)$  is now improved thanks to the EG1 experiment at JLab, which had its first data run in 2000–2001. A preliminary analysis of this data became available in 2005 [74]; final data is anticipated “soon”. The  $Q^2$  range measured in this experiment went down to  $0.05 \text{ GeV}^2$ . Using analytic forms checked against the preliminary data, Ref. [80] has evaluated  $\Delta_{\text{pol}}$  and obtained

$$\Delta_{\text{pol}}(\text{NCG 2006}) = (1.3 \pm 0.3) \text{ ppm} . \quad (52)$$

This is similar to the 2002 Faustov-Martynenko result, but with a claim that the newer data allows a smaller uncertainty limit.

A list of the numerical values of the corrections compared to the experimental value of the hfs is given in Table 1. For the polarizability corrections, we used the value from Ref. [80] on the grounds that it was based on the most complete inelastic electron-proton scattering data. For the Zemach term, we used the value [86] based on the form factor fits of Sick [87], because those fits emphasized the low- $Q^2$  elastic scattering data that dominates the Zemach integral. The values for the recoil terms and weak interaction corrections have lower uncertainty limits. We took the former from [65] and they are also discussed in [62]; the latter may be found in [62, 64].

Table 1: Up-to-date corrections to hydrogenic hyperfine structure. The first line with numbers gives the “target value” based on the experimental data and the best evaluation of the Fermi energy (8 figures) based on known physical constants. The corrections are listed next. (The Zemach term includes a 1.53% correction from higher order electronic contributions [85], as well as a +0.07 ppm correction from muonic vacuum polarization and a +0.01 ppm correction from hadronic vacuum polarization [62].) The total of all corrections is  $1.68 \pm 0.60$  ppm short of the experimental value.

Quantity	value (ppm)	uncertainty (ppm)
$(E_{\text{hfs}}(e^-p)/E_F^p) - 1$	1 103.48	0.01
$\Delta_{\text{QED}}$	1 136.19	0.00
$\Delta_Z$ (using Friar & Sick [86])	−41.59	0.46
$\Delta_R^p$	5.84	0.15
$\Delta_{\text{pol}}$ (from [80])	1.30	0.30
$\Delta_{\text{weak}}^p$	0.06	
Total	1101.80	0.60
Deficit	1.68	0.60

Thus the sum of what one may argue are the best calculated corrections falls short of the data by about 2 ppm, or about 2.8 standard deviations. Of course, some judgement has entered the choice of numbers. Other form factor fits to ostensibly the same data give



different values for  $\Delta_Z$ ; for example the form factors of Kelly [87] lead to  $\Delta_Z = -40.93 \pm 49$  ppm. The reader will surely notice that using the Kelly based value of  $\Delta_Z$  and the latest value of  $\Delta_{\text{pol}}$  from Faustov, Gorbacheva, and Martynenko leads to excellent agreement of the measured hfs.

### 3.4 Comments on the derivations of the formulas

The polarizability corrections depend on theoretical results that are obtained using unsubtracted dispersion relations. One would like to know just what this means, and since there is at least a small discrepancy between calculation and data, one would like to be able to assess the validity of such dispersion relations.

Dispersion relations[88] involve imagining some particular real variable to be a complex one and then using the Cauchy integral formula to find the functions of that variable at a particular point in terms of an integral around the boundary of some region. This is a useful thing to do because, at least in particular cases, we have information from other sources about the function on part of the boundary, and legitimate reasons for neglecting contributions from the rest of the boundary. In the present case we consider the functions  $H_i(\nu, q^2)$  and we “disperse” in  $\nu$ , treating  $q^2$  as a constant while we do so. Three things are needed to make the dispersion calculation work:

- The Cauchy formula and knowing the analytic structure (locations of poles and cuts) of the desired amplitudes.
- The optical theorem, to relate the forward Compton  $\text{Im } H_i$  to inelastic scattering cross sections.
- A reason for discarding contributions from some  $\infty$  contour, if the dispersion relation is to be “unsubtracted.”

The first two requirements are not in question.

One can consider the elastic and inelastic parts of  $H_i$  separately, but it is best to consider them together and separate the terms at the end. For  $H_1$ , one can show that it is even in  $\nu$ , so we will let the dispersion variable be  $\nu^2$  rather than  $\nu$ . The contour of integration is shown in Fig. 11, where one should imagine the outside circle having infinite radius. Along the real axis, the isolated pole corresponds to elastic scattering and the cut is for inelastic scattering kinematics. The result for  $H_1$  at some general point  $\nu^2$  begins its existence as

$$H_1(\nu, q^2) = \frac{\text{Res } H_1(\nu, q^2)|_{el}}{\nu_{el}^2 - \nu^2} + \frac{1}{\pi} \int_{cut} \frac{\text{Im } H_1(\nu', q^2)}{\nu'^2 - \nu^2} d\nu'^2 + \frac{1}{2\pi i} \int_{|\nu'|=\infty} \frac{H_1(\nu', q^2)}{\nu'^2 - \nu^2} d\nu'^2. \quad (53)$$

The numerator of the first term is the residue (Res) from the poles in  $\nu$  for the elastic part of  $H_1$ , as from Fig. 10.

We can interject here that an alternative calculation of the elastic contributions can be done directly, with no dispersion relations, simply using the photon-proton vertex given earlier (Eq. (38)), whether or not the intermediate proton is on-shell. We do not recommend doing the calculation this way, since the vertex cannot be guaranteed correct for off-shell protons, but the result is instructive. For purposes of discussion we quote the result for  $H_1$ :

$$H_1^{el} = -\frac{2M}{\pi} \left( \frac{q^2 F_1(q^2) G_M(q^2)}{(q^2 + i\epsilon)^2 - 4M^2 \nu^2} + \frac{F_2^2(q^2)}{4M^2} \right). \quad (54)$$

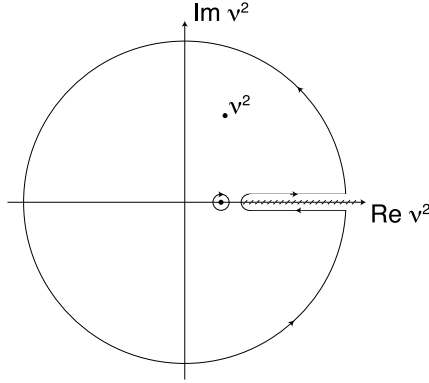


Figure 11: Contour in complex  $\nu^2$  plane for applying Cauchy identity to  $H_1$  or  $H_2$ .

One can obtain the residue for the dispersion relation from the first term above (and do so correctly, since the result is correct at the pole), and insert it into the dispersion relation to reproduce (of course) the same term. Of more interest is that the  $F_2^2$  term is constant is  $\nu$ , has no imaginary part, and is therefore absent in the dispersive calculation. Thus there is a difference, at least at the moment, between the elastic part of the result obtained from the dispersive calculation and what one finds in, for example, [67] or [68].

The second term leads to the  $g_1$  term in the quantity  $\Delta_1$  given earlier, after using the optical theorem to relate  $\text{Im } H_i$  to  $g_1$ .

The third term is the integral over the part of the contour which is the infinite radius circle. The commonly quoted results for  $\Delta_{\text{pol}}$ , which appear in this paper, depend on dropping this term. The term is zero, if  $H_1$  falls to zero at infinite  $|\nu|$ . Assuming this is true, however, appears to be a dramatic assumption. For example, if the above  $H_1^{\text{el}}$  were correct (and it could be: the oft criticized vertex in Eq. (38) is not guaranteed to be right, but neither are we aware of a guarantee that it is wrong), the assumption would fail for  $H_1^{\text{el}}$  alone. Hence, for the assumption to succeed requires an exact cancelation between elastic and inelastic contributions, or a failure of Eq. (54) on the big contour. On the positive side are several considerations. One is that nearly the same derivation gives the GDH sum rule, which is checked experimentally and works, within current experimental uncertainty (8%) [89]. Also, the GDH sum rule has been checked in lowest order and next-to-lowest order perturbation theory in QED, where it appears to work [90, 91]. Finally, Regge theory suggests the Compton amplitude does fall to zero with energy [92], as one would like, although Regge theory famously gave wrong high  $\nu$  behavior for spin-independent analogs of  $g_1$  and  $g_2$  [93]. On the other hand, parton model calculations [94] have suggested a reason why the Regge theory would fail for the spin-independent structure functions but still be correct for the spin-dependent ones. Hence there are indications, though not decisive proof, supporting the unsubtracted dispersion relation.

The dispersive derivation finishes by subtracting a term involving  $F_2^2$  from the relativistic recoil term, so as to obtain exactly the elastic corrections  $\Delta_{\text{el}} = \Delta_Z + \Delta_R^p$  that were obtained (say) by Bodwin and Yennie for a calculation of the elastic terms only, using Eq. (38) at the photon-proton vertices and no dispersion theory [67]. After adding the same term to the polarizability corrections in  $\Delta_1$ , one obtains the commonly quoted result for  $\Delta_1$  [76, 77, 79]. As noted earlier, this reorganization also allows  $\Delta_1$  to be finite in the  $m_e \rightarrow 0$  limit. Beyond the historical connection, if one is comfortable with the unsubtracted dispersion relation, the use of the dispersion theory gives a more secure

result because it uses only the pole part of the photon-proton-proton vertex, so that the combined elastic and inelastic result does not depend on the general validity of whatever photon-proton-proton vertex one uses.

### 3.5 Remarks and prospects

Thus the calculated hyperfine splitting in atomic hydrogen is an example of two-photon physics, and requires proton structure information measured at nuclear and particle physics laboratories. Until 2006, the largest uncertainty was in the proton polarizability corrections, which are related to data from polarized inelastic electron-proton scattering. The numerical value of the polarizability contributions to hydrogen hyperfine structure, based on latest proton structure function data is  $\Delta_{\text{pol}} = (1.3 \pm 0.3)$  ppm. This is quite similar to the Faustov-Martynenko 2002 result, which we think is remarkable given the improvement in the data upon which it is based. Most of the calculated  $\Delta_{\text{pol}}$  comes from integration regions where the photon four-momentum squared is small,  $Q^2 < 1 \text{ GeV}^2$ .

There is still a modest discrepancy between what we think are the best hydrogen hfs calculations and experiment, on the order of 2 ppm. Where may the problem lie? It could be in the use of the unsubtracted dispersion relation; or it could be in the value of the Zemach radius, which taken at face value now contributes the largest single uncertainty among the hadronic corrections to hfs; or perhaps it is a low  $Q^2$  surprise in  $g_1$  or  $g_2$ . It is at any rate not a statistical fluctuation in the hfs data itself.

An interplay between the fields of atomic and nuclear or particle physics may be relevant to sorting out the problem. For one example, the best values of the proton charge radius currently come from small corrections accurately measured in atomic Lamb shift [87]. The precision of the atomic measurement of the proton charge radius can increase markedly if the Lamb shift is measured in muonic hydrogen [95], and data may be taken in 2007 at the Paul Scherrer Institute. In the present context, the charge radius is noticed by its effect on determinations of the Zemach radius.

We close this section by noting that the final EG1 data analysis from JLab/CLAS should be released soon, and this may shift the value of  $\Delta_{\text{pol}}$  somewhat. We may also note that one can keep the lepton masses so as to calculate muonic hydrogen hyperfine splitting, and calculations have already appeared [84, 96].

## 4 Beam and target normal spin asymmetries

In this section we discuss the imaginary part of the two-photon exchange amplitude. It can be accessed in the beam or target normal spin asymmetries in elastic electron-nucleon scattering, and measures the non-forward structure functions of the nucleon. After briefly reviewing the theoretical formalism, we discuss calculations in the threshold region, in the resonance region, in the diffractive region, corresponding with high energy and forward angles, as well as in the hard scattering region.

The imaginary (absorptive) part of the  $2\gamma$  exchange amplitude can be accessed through a single spin asymmetry (SSA) in elastic electron-nucleon scattering, when either the target or beam spin are polarized normal to the scattering plane, as has been discussed some time ago [29, 30, 97]. As time reversal invariance forces this SSA to vanish for one-photon exchange, it is of order  $\alpha = e^2/(4\pi) \simeq 1/137$ . Furthermore, to polarize an ultra-relativistic particle in the direction normal to its momentum involves a suppression factor  $m/E$  (with  $m$  the mass and  $E$  the energy of the particle), which for the electron is of order  $10^{-4} - 10^{-3}$  when the electron beam energy is in the 1 GeV range. Therefore, the resulting target normal SSA can be expected to be of order  $10^{-2}$ , whereas the beam normal SSA is of order  $10^{-6} - 10^{-5}$ . A measurement of such small asymmetries is quite demanding experimentally. However, in the case of a polarized lepton beam, asymmetries of the order ppm are currently accessible in parity violation (PV) elastic  $eN$  scattering experiments. The parity violating asymmetry involves a beam spin polarized along its momentum. However the SSA for an electron beam spin normal to the scattering plane can also be measured using the same experimental set-ups. First measurements of this beam normal SSA at beam energies up to 1 GeV have yielded values around  $-10$  ppm [98, 99, 100] in the forward angular range and up to an order of magnitude larger in the backward angular range [101]. At higher beam energies, first results for the beam normal SSA in elastic electron-nucleon scattering experiments have also been reported recently [100, 102, 103].

First estimates of the target normal SSA in elastic electron-nucleon scattering have been performed in [30, 97]. In those works, the  $2\gamma$  exchange with nucleon intermediate state (so-called elastic or nucleon pole contribution) has been calculated, and the inelastic contribution has been estimated in a very forward angle approximation. Estimates within this approximation have also been reported for the beam normal SSA [104]. The general formalism for elastic electron-nucleon scattering with lepton helicity flip, which is needed to describe the beam normal SSA, has been developed in [105]. Furthermore, the beam normal SSA has also been estimated at large momentum transfers  $Q^2$  in [105] using a parton model, which was found crucial [36] to interpret the results from unpolarized electron-nucleon elastic scattering, as discussed in Section 2. In the handbag model of Refs. [36, 37, 105], the corresponding  $2\gamma$  exchange amplitude has been expressed in terms of generalized parton distributions, and the real and imaginary part of the  $2\gamma$  exchange amplitude are related through a dispersion relation. Hence in the partonic regime, a direct comparison of the imaginary part with experiment can provide a very valuable cross-check on the calculated result for the real part.

To use the elastic electron-nucleon scattering at low momentum transfer as a high precision tool, such as in present day PV experiments, one may also want to quantify the  $2\gamma$  exchange amplitude. To this aim, one may envisage a dispersion formalism for the elastic electron-nucleon scattering amplitudes, as has been discussed some time ago in the literature [56, 55]. To develop this formalism, the necessary first step is a precise knowledge of the imaginary part of the two-photon exchange amplitude, which enters

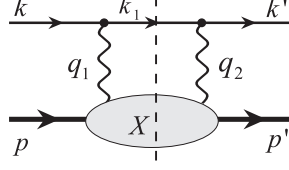


Figure 12: The two-photon exchange diagram. The filled blob represents the response of the nucleon to the scattering of the virtual photon. In the imaginary part of the two-photon amplitude, the intermediate state indicated by the vertical dashed line is on-shell.

in both the beam and target normal SSA. Using unitarity, one can relate the imaginary part of the  $2\gamma$  amplitude to the electro-absorption amplitudes on a nucleon, see Fig. 12.

#### 4.1 Single spin asymmetries in elastic electron-nucleon scattering

An observable which is directly proportional to the imaginary part of the two- (or multi-) photon exchange is given by the elastic scattering of an unpolarized electron on a proton target polarized *normal* to the scattering plane (or the recoil polarization normal to the scattering plane, which is exactly the same assuming time-reversal invariance). For a target polarized perpendicular to the scattering plane, the corresponding single spin asymmetry, which we refer to as the target normal spin asymmetry ( $A_n$ ), is defined by :

$$A_n = \frac{\sigma_{\uparrow} - \sigma_{\downarrow}}{\sigma_{\uparrow} + \sigma_{\downarrow}}, \quad (55)$$

where  $\sigma_{\uparrow}$  ( $\sigma_{\downarrow}$ ) denotes the cross section for an unpolarized beam and for a nucleon spin parallel (anti-parallel) to the normal polarization vector, defined as :

$$S_n^{\mu} = (0, \vec{S}_n), \quad \vec{S}_n \equiv (\vec{k} \times \vec{k}') / |\vec{k} \times \vec{k}'|. \quad (56)$$

As has been shown by de Rujula *et al.* [30], the target (or recoil) normal spin asymmetry is related to the absorptive part of the elastic  $eN$  scattering amplitude as :

$$A_n = \frac{2 \text{Im}(\sum_{spins} T_{1\gamma}^* \cdot \text{Abs } T_{2\gamma})}{\sum_{spins} |T_{1\gamma}|^2}, \quad (57)$$

where  $T_{1\gamma}$  denotes the one-photon exchange amplitude. Since the one-photon exchange amplitude is purely real, the leading contribution to  $A_n$  is of order  $O(e^2)$ , and is due to an interference between one- and two-photon exchange amplitudes. When neglecting terms which correspond with electron helicity flip (i.e. setting  $m_e = 0$ ),  $A_n$  can be expressed in terms of the invariants for electron-nucleon elastic scattering, defined in Eq. (9) as [36] :

$$A_n = \sqrt{\frac{2\varepsilon(1+\varepsilon)}{\tau}} \left( G_M^2 + \frac{\varepsilon}{\tau} G_E^2 \right)^{-1} \times \left\{ -G_M \mathcal{I} \left( \delta \tilde{G}_E + \frac{\nu}{M^2} \tilde{F}_3 \right) + G_E \mathcal{I} \left( \delta \tilde{G}_M + \left( \frac{2\varepsilon}{1+\varepsilon} \right) \frac{\nu}{M^2} \tilde{F}_3 \right) \right\} + \mathcal{O}(e^4), \quad (58)$$

where  $\mathcal{I}$  denotes the imaginary part.

For a beam polarized perpendicular to the scattering plane, one can also define a single spin asymmetry, analogously as in Eq. (55) as noted in Ref. [104], where now  $\sigma_{\uparrow}$  ( $\sigma_{\downarrow}$ ) denotes the cross section for an unpolarized target and for an electron beam spin parallel (anti-parallel) to the normal polarization vector, given by Eq. (56). We refer to this asymmetry as the beam normal spin asymmetry ( $B_n$ ). It explicitly vanishes when  $m_e = 0$  as it involves an electron helicity flip. The general electron-nucleon scattering amplitude including lepton helicity flip involves six invariant amplitudes and has been worked out in Ref. [105], where the expression for  $B_n$  can also be found. As for  $A_n$ , also  $B_n$  vanishes in the Born approximation, and is therefore of order  $e^2$ .

## 4.2 Imaginary (absorptive) part of the two-photon exchange amplitude

In this section we discuss the relation between the imaginary part of the two-photon exchange amplitude and the absorptive part of the doubly virtual Compton scattering tensor on the nucleon, as shown in Fig. 12.

The discontinuity of the two-photon exchange amplitude, shown in Fig. 12, can then be expressed as :

$$\text{Abs}T_{2\gamma} = e^4 \int \frac{d^3\vec{k}_1}{(2\pi)^3 2E_{k_1}} \bar{u}(k', h') \gamma_{\mu} (\gamma \cdot k_1 + m_e) \gamma_{\nu} u(k, h) \cdot \frac{1}{Q_1^2 Q_2^2} \cdot W^{\mu\nu}(p', \lambda'_N; p, \lambda_N), \quad (59)$$

where the momenta are defined as indicated on Fig. 12, with  $q_1 \equiv k - k_1$ ,  $q_2 \equiv k' - k_1$ , and  $q_1 - q_2 = q$ . Here  $h(h')$  denote the helicities of the initial (final) electrons and  $\lambda_N(\lambda'_N)$  denote the helicities of the initial (final) nucleons. In Eq. (59), the hadronic tensor  $W^{\mu\nu}(p', \lambda'_N; p, \lambda_N)$  corresponds with the absorptive part of the doubly virtual Compton scattering tensor with two *space-like* photons :

$$W^{\mu\nu}(p', \lambda'_N; p, \lambda_N) = \sum_X (2\pi)^4 \delta^4(p + q_1 - p_X) \langle p', \lambda'_N | J^{\dagger\mu}(0) | X \rangle \langle X | J^{\nu}(0) | p, \lambda_N \rangle, \quad (60)$$

where the sum goes over all possible *on-shell* intermediate hadronic states  $X$  (denoting  $p_X^2 \equiv W^2$ ). Note that in the limit  $p' = p$ , Eq. (60) reduces to the forward tensor for inclusive electron-nucleon scattering and can be parametrized by the usual 4 nucleon forward structure functions. In the non-forward case however, the absorptive part of the doubly virtual Compton scattering tensor of Eq. (60) which enters in the evaluation of target and beam normal spin asymmetries, depends upon 18 invariant amplitudes [106]. Though this may seem as a forbiddingly large number of new functions, we may use the unitarity relation to express the full non-forward tensor in terms of electroproduction amplitudes  $\gamma^* N \rightarrow X$ . The number of intermediate states  $X$  which one considers in the calculation will then put a limit on how high in energy one can reliably calculate the hadronic tensor Eq. (60). In the following section, the tensor  $W^{\mu\nu}$  will be discussed for the elastic contribution ( $X = N$ ), in the resonance region as a sum over all  $\pi N$  intermediate states (i.e.  $X = \pi N$ ), using a phenomenological state-of-the-art calculation for the  $\gamma^* N \rightarrow \pi N$  amplitudes, in the diffractive region (corresponding with high energy, forward scattering) where it can be related to the total photo-absorption cross section on a proton, as well as in the hard scattering region where it can be related to nucleon generalized parton distributions.



There are special regions in the phase space integral of Eq. (59), corresponding with near singularities, which may give important contributions (logarithmic enhancements) under some kinematical conditions. When the intermediate and initial electrons are collinear, then also the photon with momentum  $\vec{q}_1$  is collinear with this direction. For the elastic case ( $W = M$ ) this precisely corresponds with the situation where the first photon is soft (i.e.  $q_1 \rightarrow 0$ ) and where the second photon carries the full momentum transfer  $Q_2^2 \simeq Q^2$ . For the inelastic case ( $W > M$ ) the first photon is hard but becomes quasi-real (i.e.  $Q_1^2 \sim m_e^2$ ). In this case, the virtuality of the second photon is smaller than  $Q^2$ . An analogous situation occurs when the intermediate electron is collinear with the final electron. These kinematical situations with one quasi-real photon and one virtual photon correspond with quasi virtual Compton scattering (quasi-VCS). Besides the quasi-VCS singularities, the two-photon exchange amplitude also has a near singularity when the intermediate electron momentum is soft (i.e.  $|\vec{k}_1| \rightarrow 0$ ). In this case both photons are hard but have virtualities which become very small, and vanish if the electron mass is taken to zero. This situation, with two quasi-real photons, occurs when the invariant mass of the hadronic state takes on its maximal value  $W_{max} = \sqrt{s} - m_e$ , and corresponds to quasi-real Compton scattering (quasi-RCS).

## 4.3 Results and discussion

### 4.3.1 Threshold region

In Ref. [107], the beam normal spin asymmetry was studied at low energies in an effective theory of electrons, protons and photons. This calculation, in which pions are integrated out, effectively corresponds with the nucleon intermediate state contribution only, expanded to second order in  $E_e/M$ . To this order, the calculation includes the recoil corrections to the scattering from a point charge, the nucleon charge radius, and the nucleon isovector magnetic moment. One sees from Fig. 13 (right panel) that the theory expanded up to second order in  $E_e/M$  (indicated by the full results) is able to give a good account of the SAMPLE data point at the low energy  $E_e = 0.2$  GeV.

However, when doing the full calculation for the  $N$  intermediate state, which is model independent (as it only involves on-shell  $\gamma^*NN$  matrix elements), the result is further reduced as seen in Fig. 13 (left panel). Inclusion of threshold pion electroproduction contributions, arising from the  $\pi N$  intermediate states, partly cancels the elastic contributions. Because in this low-energy region, the matrix elements are rather well known, it is not clear at present how to get a better agreement with the rather large asymmetry measured by SAMPLE [98].

### 4.3.2 Resonance region

When measuring the imaginary part of the elastic  $eN$  amplitude through a normal SSA at sufficiently low energies, below or around two-pion production threshold, one is in a regime where these electroproduction amplitudes are relatively well known using pion electroproduction experiments as input. As both photons in the  $2\gamma$  exchange process are virtual and integrated over, an observable such as the beam or target normal SSA is sensitive to the electroproduction amplitudes on the nucleon for a range of photon virtualities. This may provide information on resonance transition form factors complementary to the information obtained from current pion electroproduction experiments.

In Ref. [108], the imaginary part of the two-photon exchange amplitude was calculated



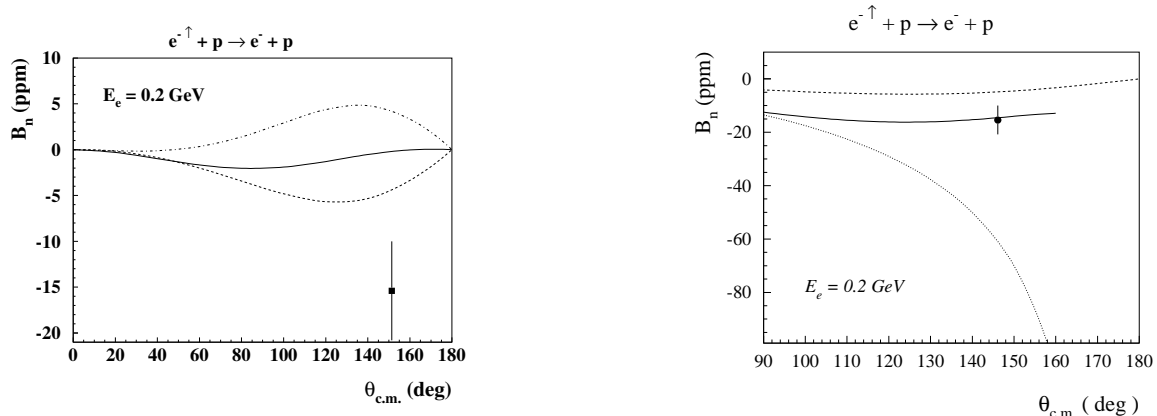


Figure 13: Beam normal spin asymmetry for  $e^-p \rightarrow e^-p$  at a beam energy  $E_e = 0.2$  GeV as function of the  $c.m.$  scattering angle. Left panel : calculation from Ref. [108] for different hadronic intermediate states ( $X$ ) in the blob of Fig. 12 :  $N$  (dashed curve),  $\pi N$  (dashed-dotted curve), sum of the  $N$  and  $\pi N$  (solid curve). Right panel : calculation of Ref. [107], where the nucleon intermediate state is expanded to leading order (dotted curve) and next to leading order (solid curve) in  $E_e/M$ . For comparison, also the full nucleon intermediate state result (dashed curve, same as on left panel) is shown. The data point is from the SAMPLE Coll. [98].

by relating it through unitarity to the contribution of  $X = N$  and  $X = \pi N$  intermediate state contributions. For the  $\pi N$  intermediate state contribution, the corresponding pion electroproduction amplitudes were taken from the phenomenological MAID analysis [109], which contains both resonant and non-resonant pion production mechanisms. The calculation of [108] shows that at forward angles, the quasi-real Compton scattering at the endpoint  $W = W_{max}$  only yields a very small contribution, which grows larger when going to backward angles. This quasi-RCS contribution is of opposite sign as the remainder of the integrand, and therefore determines the position of the maximum (absolute) value of  $B_n$  when going to backward angles.

In Fig. 14, the results for  $B_n$  are shown at different beam energies below  $E_e = 1$  GeV. It is clearly seen that at energies  $E_e = 0.3$  GeV and higher the nucleon intermediate state (elastic part) yields only a very small relative contribution. Therefore  $B_n$  is a direct measure of the inelastic part which gives rise to sizeable large asymmetries, of the order of several tens of ppm in the backward angular range, mainly driven by the quasi-RCS near singularity. First results from the A4 Coll. for  $B_n$  at backward angles (for  $E_e$  around 0.3 GeV) indeed point towards a large  $B_n$  value of order -100 ppm for  $\theta_{cm}$  around 150 deg [101]. At forward angles, the sizes of the predicted asymmetries are compatible with the first high precision measurements performed by the A4 Coll. [99], though the model slightly overpredicts (in absolute value)  $B_n$  at  $E_e = 0.570$  GeV and 0.855 GeV.

#### 4.3.3 High-energy, forward scattering (diffractive) region

At very high energies and forward scattering angles (so-called diffractive limit), it was shown in Refs. [110, 111] that  $B_n$  is dominated by the quasi-real Compton singularity. In

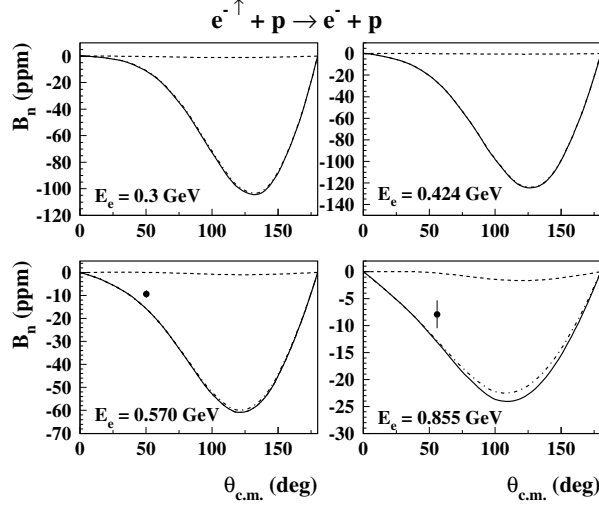


Figure 14:  $B_n$  for  $e^-p \rightarrow e^-p$  as function of the *c.m.* scattering angle at different beam energies, as indicated on the figure. The calculations are for different hadronic intermediate states ( $X$ ) in the blob of Fig. 12 :  $N$  (dashed curve),  $\pi N$  (dashed-dotted curves), sum of the  $N$  and  $\pi N$  (solid curves). The data points are from the A4 Coll. (MAMI) [99]. Calculations and figure from Ref. [108].

this (extreme forward limit) case, the hadronic tensor can be expressed in terms of the total photo-absorption cross section on the proton,  $\sigma_{tot}^{\gamma p}$ , allowing to express  $B_n$  through the simple analytic expression :

$$B_n = -\frac{m_e \sqrt{Q^2} \sigma_{tot}^{\gamma p}}{8\pi^2} \frac{G_E}{\tau G_M^2 + \varepsilon G_E^2} \left[ \log \frac{Q^2}{m_e^2} - 2 \right]. \quad (61)$$

One notices that the quasi-real Compton singularity gives rise to a (single) logarithmic enhancement factor which is at the origin of the relatively large value of  $B_n$ .

In Fig. 15, the estimate from Ref. [110] based on Eq. (61) is shown for different parameterizations of the total photo-absorption cross section. The beam normal spin asymmetry has been measured at SLAC (E-158) at an energy  $E_e = 46$  GeV ( $\sqrt{s} \simeq 9$  GeV) and very forward angle ( $Q^2 \simeq 0.05 \text{ GeV}^2$ ). First result [102] indicate a value  $B_n \simeq -3.5 \rightarrow -2.5$  ppm, confirming the estimate shown in Fig. 15.

At intermediate energies, around  $E_e \simeq 3$  GeV, and forward angles,  $B_n$  has also been measured by the HAPPEX and G0 Collaborations. The simple “diffractive” formula of Eq. (61) does not rigorously apply any more and one has to calculate corrections due to the deviation from forward scattering. Such calculation have recently been performed in Refs. [110, 112] in different model approaches, where the calculation of Ref. [112] includes subleading terms in  $Q^2$ . The predicted asymmetries are in basic agreement with first results reported by HAPPEX [100] and G0 [103].

In Table 2, the present status of measurements of beam normal spin asymmetries, most of them in the forward angular range, is shown.

#### 4.3.4 Hard scattering region

In the hard scattering region, the beam and target normal spin asymmetries were estimated in Refs. [105, 37] through the scattering off a parton, which is embedded in the

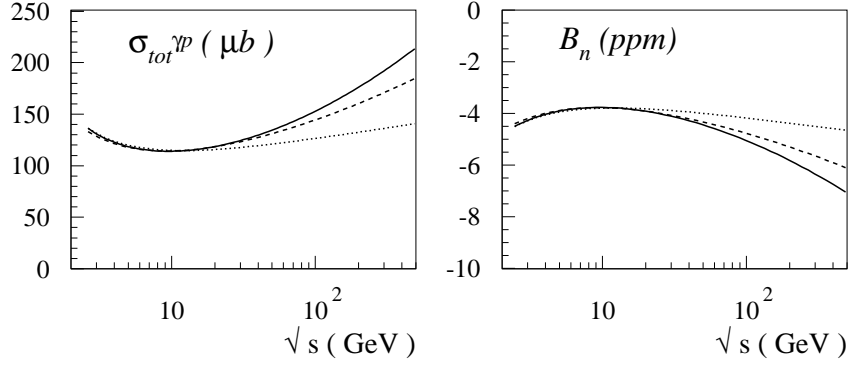


Figure 15: Energy dependence of  $B_n$  for  $e^-p \rightarrow e^-p$  (right panel) at  $Q^2 = 0.05 \text{ GeV}^2$  (corresponding with very forward scattering angle) using Eq. (61) for different parameterizations of the total photo-absorption cross section on the proton (left panel) : Block-Halzen  $\log$  fit (dotted curves), Block-Halzen  $\log^2$  fit (solid curves), and Donnachie-Landshoff fit (dashed curves). Calculations from Ref. [110].

Table 2: Summary of measurements of the beam normal spin asymmetry in elastic electron-proton scattering

EXP.	$E_e$ (GeV)	$Q^2$ (GeV $^2$ )	$B_n$ (ppm)
SAMPLE [98]	0.192	0.10	$-16.4 \pm 5.9$
A4 [99]	0.570	0.11	$-8.59 \pm 0.89$
A4 [99]	0.855	0.23	$-8.52 \pm 2.31$
HAPPEX [100]	3.0	0.11	$-6.7 \pm 1.5$
G0 [103]	3.0	0.15	$-4.04 \pm 1.05$
G0 [103]	3.0	0.25	$-4.81 \pm 2.03$
E-158 [102]	46	0.06	$-3.5 \rightarrow -2.5$

nucleon through a GPD.

The GPD estimate for the target spin asymmetry  $A_n$  for the proton is shown in the left-hand plot of Fig. 16 as a function of the CM scattering angle for fixed incoming electron lab energy, taken here as 6 GeV. Also shown is a calculation of  $A_n$  including the elastic intermediate state only [30]. The result, which is nearly the same for either of the two GPD parameterizations which were used in Ref. [37], is of order 1%. Fig. 16 on the right also shows a similar plot of  $A_n$  for a neutron target. The predicted asymmetry is of opposite sign, reflecting that the numerically largest term in Eq. (58) is the one proportional to  $G_M$ . The results are again of order 1% in magnitude, though somewhat larger for the neutron than for the proton. A precision measurement of  $A_n$  is planned at JLab [113] on a polarized  $^3\text{He}$  target; it will provide access to the elastic electron-neutron single-spin asymmetry from two-photon exchange.

Using the same phenomenological parametrizations for the GPDs,  $B_n$  was found to yield values around +1 ppm to +1.5 ppm in the few GeV beam energy range, see Fig. 17. In particular, the forward angular range for  $e^-p \rightarrow e^-p$  scattering was found to be a favorable region to get information on the inelastic part of  $B_n$ . Because in the handbag

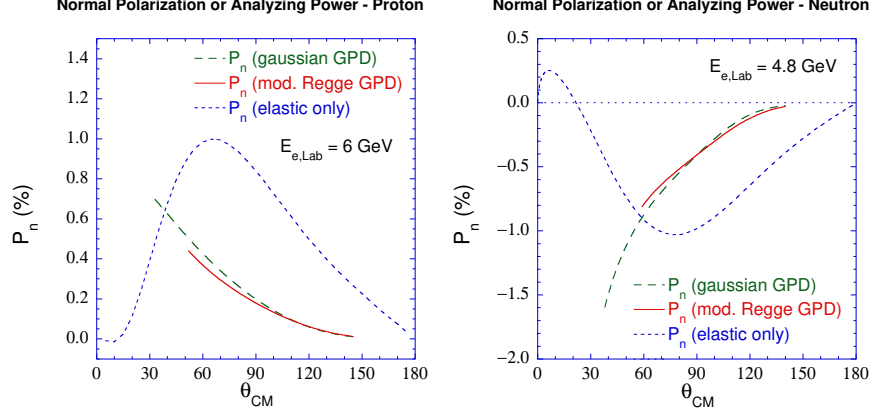


Figure 16: Nucleon analyzing power  $A_n$ , which is equal to the normal polarization  $P_n$ . The elastic contribution is shown by the dotted curve [30]. The GPD calculation for the inelastic contribution is shown by the dashed curve for a gaussian GPD model, and by the solid curve for a modified Regge GPD parameterization. The GPD calculation is cut off in the backward direction at  $-u = M^2$ . In the forward direction it goes down to  $Q^2 = 2 \text{ GeV}^2$  (modified Regge GPD) and to  $Q^2 = M^2$  (Gaussian GPD). Figure from [37].

calculation, real and imaginary parts are linked, a direct measurement of  $B_n$  may yield a valuable cross-check for the real part, which was found crucial in understanding the unpolarized cross section data for  $e^-p \rightarrow e^-p$  at large momentum transfer.

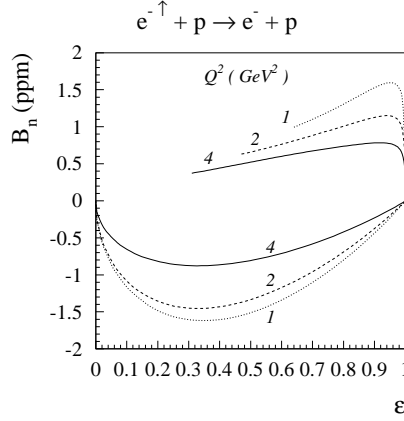


Figure 17:  $B_n$  for elastic  $e^-p$  scattering as function of  $\varepsilon$  at different values of  $Q^2$  as indicated on the figure. The upper thick curves ( $B_n > 0$ ) are the GPD calculations for the kinematical range where  $s, -u > M^2$ . For comparison, the elastic contribution is also displayed : lower thin curves ( $B_n < 0$ ). Calculations and figure from Ref. [105].

## 5 Conclusions and open issues

The striking difference between the unpolarized (Rosenbluth) and polarization transfer measurements of the proton  $G_E/G_M$  form factor ratio has triggered a renewed interest in the field of two-photon exchange in electron-nucleon scattering experiments. Theoretical calculations both within a hadronic and partonic framework, which were reviewed in this work, made it very likely that hard two-photon exchange corrections are the main culprit in the difference between both experimental techniques. Despite the long history of two-photon exchange corrections, it is interesting to note that concepts developed over the past decade, such as generalized parton distributions which describe two-photon processes with one or two large photon virtualities, enter when quantifying two-photon exchange corrections at larger  $Q^2$ .

The model-independent finding is that the hard two-photon corrections hardly affect polarization transfer results, but they do correct the slope of the Rosenbluth plots at larger  $Q^2$  in an important way, towards reconciling the Rosenbluth data with the  $G_E/G_M$  ratio, which decreases linearly in  $Q^2$ , from the polarization data. This being said, it is fair to state at this point that neither of the current calculations convincingly quantifies the effect either due to uncontrolled approximations (such as using ad hoc assumptions for off-shell vertices in hadronic calculations), or extrapolations beyond their region of validity (such as applying partonic calculations in the low momentum transfer regime). The present and forthcoming high-precision electron scattering data, which aim at testing two-photon exchange effects, have shifted the emphasis, however, from the qualitative to the quantitative realm.

Besides entering as corrections to elastic electron-nucleon scattering data, two-photon exchange processes are also the leading corrections to improve our quantitative understanding of the hyperfine splitting (hfs) in hydrogen. We reviewed in this work that our best estimate, based on the recent data for polarized nucleon structure functions which enter the polarizability correction to the hydrogen hfs, yields a result  $\Delta_{pol} = (1.3 \pm 0.3)$  ppm. Combined with recent estimates of the Zemach radius, the correction to the hydrogen hfs falls short of the data by about 2 ppm, or about 2.8 standard deviations.

We have also reviewed the recent measurements of large beam normal single spin asymmetries (SSA), of order  $-10$  to  $-100$  ppm, and measured with ppm level accuracy, which arose over the past few years as an interesting spin-off of the high precision parity violation experiments in electron-nucleon scattering. We discussed how such asymmetries, which measure the imaginary part of the two-photon exchange amplitude, can be expressed through non-forward nucleon structure functions and provide a new tool to access hadron structure information.

We end this review by spelling out a few open issues and challenges (both theoretical and experimental) in this field :

### 1. *Experimental measurements of the two-photon exchange processes*

In order to use electron scattering as a precision tool, it is clearly worthwhile to arrive at a quantitative understanding of two-photon exchange processes. This calls for detailed experimental studies, and several new experiments are already planned. A first type of experiments is to perform high precision unpolarized experiments and look for nonlinearities in the Rosenbluth plots. A recent study [114] found that the non-linearities in  $\epsilon$  in current Rosenbluth data stay small over a fairly large  $Q^2$  range. Such experiments however cannot separate that part of the

two-photon corrections which is linear in  $\varepsilon$  and which appears to be the dominant source of corrections in theoretical calculations. The difference between elastic  $e^-$  and  $e^+$  scattering on a proton target directly accesses the real part of the two-photon exchange amplitude and the part linear in  $\varepsilon$ . At intermediate  $Q^2$  values some forthcoming  $e^+/e^-$  experiments at JLab [50] and VEPP-3 [115] will allow one to systematically study and quantify two-photon exchange effects. Also forthcoming is an experimental check of the predicted small effect of two-photon processes on the polarization data by measuring the  $\varepsilon$  dependence in polarization transfer experiments [49].

2. *Further refinements on the theoretical side : real part of the two-photon exchange amplitude*

The calculations of the real part of the two-photon amplitude for elastic  $eN$  scattering described in this work are performed either within a hadronic framework at lower  $Q^2$  values or partonic picture at larger  $Q^2$  values. The hadronic calculation assumes some off-shell vertex functions and performs a four-dimensional integral of the box diagram. It would be desirable to have a dispersion relation framework where the real part is explicitly calculated as an integral over the imaginary part, which can be related to observables (*i.e.* on-shell amplitudes) using unitarity. In the forward limit such dispersion relations are underlying, *e.g.*, the evaluation of the hyperfine splitting in hydrogen. In the non-forward case, the convergence of such dispersion relations would need further study. Within the partonic framework, a full calculation of the processes with two-active quarks (the so-called cat's ears diagrams) remains to be performed.

3. *Systematic exploration of the imaginary part of the two-photon exchange amplitude*

The ongoing experiments for both the beam and target normal SSA in elastic  $eN$  scattering will trigger further theoretical work, and a cross-fertilization between theory and experiment can be expected in this field.

4. *Two-photon exchange effects in resonance production processes*

The sensitivity of unpolarized measurements of  $G_E/G_M$  to two-photon exchange effects also signals that such potential effects can be expected when measuring resonance transition form factors out to larger  $Q^2$  values as is performed, *e.g.*, at JLab. In particular a first theoretical study of the two-photon exchange contribution to the  $eN \rightarrow e\Delta(1232) \rightarrow e\pi N$  process with the aim of a precision study of the ratios of electric quadrupole (E2) and Coulomb quadrupole (C2) to the magnetic dipole (M1)  $\gamma^*N\Delta$  transitions, has been recently performed [116]. The two-photon exchange amplitude has been related to the  $N \rightarrow \Delta$  GPDs. It was found that the C2/M1 ratio at larger  $Q^2$  values depends strongly on whether this quantity is obtained from an interference cross section or from the Rosenbluth-type cross sections, in similarity with the elastic,  $eN \rightarrow eN$ , process. It will be interesting to confront these results with upcoming new Rosenbluth separation data at intermediate  $Q^2$  values in order to arrive at a precision extraction of the large  $Q^2$  behavior of the  $R_{EM}$  and  $R_{SM}$  ratios.

5. *Two-photon exchange effects in deep-inelastic scattering processes*

Two-photon exchange effects were also studied in the past in deep-inelastic scattering processes; see, *e.g.*, Refs. [117, 118, 119]. They can be expected to affect

the extraction of the longitudinal structure function from  $L/T$  Rosenbluth type experiments in the deep-inelastic scattering region, which remains to be quantified.

6. *Two-photon exchange effects in parity violating elastic electron-nucleon scattering and related study of  $\gamma Z$  box diagram effects*

In recent years an unprecedented precision has been achieved in parity violating electron scattering experiments. Two-photon exchange processes may be relevant in the interpretation of the current generation of high precision parity-violation experiments, in particular for using those data to determine the strange-quark content of the proton; for a first study see Ref. [59].

A related issue in the interpretation of parity violating electron scattering experiments are the  $\gamma Z$  box diagram contributions. Such calculations have been performed for atomic parity violation [120] corresponding with zero momentum transfer as well as in the deep-inelastic scattering region [121], by calculation the  $\gamma Z$  exchange between an electron and a quark. A full calculation in the small and intermediate  $Q^2$  regime, where many current parity violation experiments are performed is definitely a worthwhile topic for further research.

7. *Two-photon exchange effects in hydrogen hyperfine splitting*

More accurate data, and data at lower  $Q^2$ , is forthcoming on polarized inelastic  $e-p$  scattering. These data will allow a more precise evaluation of the polarizability corrections to hydrogen hfs. In addition, a measurement of hfs in muonic hydrogen may be possible [95]. The calculated corrections for muonic hydrogen have different weightings because of the muon mass, and with calculations such as [80, 84, 96] updated with new scattering data, the result of the measurement could be presented as an independent accurate determination of the proton's Zemach radius.

## Acknowledgements

We like to thank A. Afanasev, S. Brodsky, Y.C. Chen, M. Gorchtein, K. Griffioen, P. Guichon, V. Nazaryan, V. Pascalutsa, and B. Pasquini for several collaborations on the subjects reviewed in this work. Furthermore we would like to thank A. Afanasev, D. Armstrong, T. Averett, L. Capozza, M. Gorchtein, F. Maas, Ch. Perdrisat, and M. Ramsey-Musolf for discussions and correspondence during the course of this work.

The work of C. E. C. is supported by the National Science Foundation under grant PHY-0555600. The work of M. V. is supported in part by DOE grant DE-FG02-04ER41302 and contract DE-AC05-06OR23177 under which Jefferson Science Associates operates the Jefferson Laboratory.



## References

- [1] C. E. Hyde-Wright and K. de Jager, *Ann. Rev. Nucl. Part. Sci.* **54**, 217 (2004).
- [2] J. Arrington, C. D. Roberts and J. M. Zanotti, arXiv:nucl-th/0611050.
- [3] C. F. Perdrisat, V. Punjabi and M. Vanderhaeghen, arXiv:hep-ph/0612014.
- [4] A.I. Akhiezer, L.N. Rosentsweig, I.M. Shmushkevich, *Sov. Phys. JETP* **6**, 588 (1958); J. Scofield, *Phys. Rev.* **113**, 1599 (1959); *ibid.* **141**, 1352 (1966); N. Dombey, *Rev. Mod. Phys.* **41**, 236 (1969); A. I. Akhiezer and M. P. Rekalo, *Sov. J. Part. Nucl.* **4**, 277 (1974); R. G. Arnold, C. E. Carlson and F. Gross, *Phys. Rev. C* **23**, 363 (1981).
- [5] M. K. Jones *et al.* [Jefferson Lab Hall A Coll.], *Phys. Rev. Lett.* **84**, 1398 (2000).
- [6] O. Gayou *et al.* [Jefferson Lab Hall A Coll.], *Phys. Rev. Lett.* **88**, 092301 (2002).
- [7] V. Punjabi *et al.*, *Phys. Rev. C* **71**, 055202 (2005) [Erratum-*ibid.* *C* **71**, 069902 (2005)].
- [8] L. Andivahis *et al.*, *Phys. Rev. D* **50**, 5491 (1994).
- [9] M. E. Christy *et al.* [E94110 Coll.], *Phys. Rev. C* **70**, 015206 (2004).
- [10] I. A. Qattan *et al.*, *Phys. Rev. Lett.* **94**, 142301 (2005).
- [11] J. Mar *et al.*, *Phys. Rev. Lett.* **21**, 482 (1968).
- [12] S. Hartwig *et al.*, *Lett. Nuovo Cim.* **12**, 30 (1975).
- [13] L. W. Mo and Y. S. Tsai, *Rev. Mod. Phys.* **41**, 205 (1969).
- [14] N. Meister and D. R. Yennie, *Phys. Rev.* **130**, 1210 (1963).
- [15] S. D. Drell and M. A. Ruderman, *Phys. Rev.* **106**, 561 (1957).
- [16] S. D. Drell and S. Fubini, *Phys. Rev.* **113**, 741 (1959).
- [17] N. R. Werthamer and M. A. Ruderman, *Phys. Rev.* **123**, 1005 (1961).
- [18] G. K. Greenhut, *Phys. Rev.* **184**, 1860 (1969).
- [19] P. A. M. Guichon and M. Vanderhaeghen, *Phys. Rev. Lett.* **91**, 142303 (2003).
- [20] J. Arrington, *Phys. Rev. C* **69**, 032201 (2004); *Phys. Rev. C* **71**, 015202 (2005).
- [21] X. D. Ji, *J. Phys. G* **24**, 1181 (1998).
- [22] K. Goeke, M. V. Polyakov and M. Vanderhaeghen, *Prog. Part. Nucl. Phys.* **47**, 401 (2001).
- [23] M. Diehl, *Phys. Rept.* **388**, 41 (2003).
- [24] X. D. Ji, *Ann. Rev. Nucl. Part. Sci.* **54**, 413 (2004).

- [25] A. V. Belitsky and A. V. Radyushkin, Phys. Rept. **418**, 1 (2005).
- [26] M. I. Eides, H. Grotch and V. A. Shelyuto, Phys. Rept. **342**, 63 (2001).
- [27] S. G. Karshenboim, Phys. Rept. **422**, 1 (2005).
- [28] G. Feinberg, J. Sucher and C. K. Au, Phys. Rept. **180**, 83 (1989).
- [29] A.O. Barut and C. Fronsdal, Phys. Rev. **120**, 1871 (1960).
- [30] A. De Rujula, J. M. Kaplan and E. De Rafael, Nucl. Phys. B **35**, 365 (1971).
- [31] P. G. Blunden, W. Melnitchouk and J. A. Tjon, Phys. Rev. Lett. **91**, 142304 (2003).
- [32] P. G. Blunden, W. Melnitchouk and J. A. Tjon, Phys. Rev. C **72**, 034612 (2005).
- [33] S. Kondratyuk, P. G. Blunden, W. Melnitchouk and J. A. Tjon, Phys. Rev. Lett. **95**, 172503 (2005).
- [34] S. Kondratyuk and P. G. Blunden, arXiv:nucl-th/0701003.
- [35] D. Borisjuk and A. Kobushkin, Phys. Rev. C **74**, 065203 (2006); arXiv:nucl-th/0612104.
- [36] Y. C. Chen, A. Afanasev, S. J. Brodsky, C. E. Carlson and M. Vanderhaeghen, Phys. Rev. Lett. **93**, 122301 (2004).
- [37] A. V. Afanasev, S. J. Brodsky, C. E. Carlson, Y. C. Chen and M. Vanderhaeghen, Phys. Rev. D **72**, 013008 (2005).
- [38] Allan S. Krass, Phys. Rev. **125**, 2172 (1962).
- [39] R. Ent, B. W. Filippone, N. C. R. Makins, R. G. Milner, T. G. O'Neill and D. A. Wasson, Phys. Rev. C **64**, 054610 (2001).
- [40] M.L. Goldberger, Y. Nambu and R. Oehme, Ann. of Phys. **2**, 226 (1957).
- [41] M. P. Rekalo and E. Tomasi-Gustafsson, Eur. Phys. J. A **22**, 331 (2004).
- [42] P. Van Nieuwenhuizen, Nucl. Phys. B **28**, 429 (1971).
- [43] G. J. Grammer and D. R. Yennie, Phys. Rev. D **8**, 4332 (1973).
- [44] S. J. Brodsky and J. R. Primack, Annals Phys. **52**, 315 (1969).
- [45] L. C. Maximon and J. A. Tjon, Phys. Rev. C **62**, 054320 (2000).
- [46] M. Guidal, M. V. Polyakov, A. V. Radyushkin and M. Vanderhaeghen, Phys. Rev. D **72**, 054013 (2005).
- [47] M. Diehl, T. Feldmann, R. Jakob and P. Kroll, Eur. Phys. J. C **39**, 1 (2005).
- [48] E. J. Brash, A. Kozlov, S. Li and G. M. Huber, Phys. Rev. C **65**, 051001 (2002).
- [49] JLab experiment E-04-019, spokespersons R. Gilman, L. Pentchev, C. Perdrisat, and R. Suleiman.

- [50] Jefferson Lab experiment E-04-116; contact person, W. Brooks.
- [51] Yu. M. Bystritskiy, E. A. Kuraev and E. Tomasi-Gustafsson, arXiv:hep-ph/0603132.
- [52] The calculated result at  $6 \text{ GeV}^2$  was presented by A. Afanasev at the Workshop on Precision ElectroWeak Interactions held at William and Mary, Williamsburg, VA, USA, 15-17 August 2005. The related calculation of hard bremsstrahlung effects in the polarized case was presented in A. Afanasev, I. Akushevich and N. Merenkov, Phys. Rev. D **64**, 113009 (2001).
- [53] Y. B. Dong, C. W. Kao, S. N. Yang and Y. C. Chen, Phys. Rev. C **74**, 064006 (2006).
- [54] M. P. Rekalo, E. Tomasi-Gustafsson and D. Prout, Phys. Rev. C **60**, 042202 (1999).
- [55] J. Bordes, J. A. Penarrocha and J. Bernabeu, Phys. Rev. D **35**, 3310 (1987).
- [56] J. A. Penarrocha and J. Bernabeu, Annals Phys. **135**, 321 (1981).
- [57] J. Bernabeu and J. A. Penarrocha, Phys. Rev. D **22**, 1082 (1980).
- [58] J. Arrington and I. Sick, arXiv:nucl-th/0612079.
- [59] A. V. Afanasev and C. E. Carlson, Phys. Rev. Lett. **94**, 212301 (2005).
- [60] P. G. Blunden and I. Sick, Phys. Rev. C **72**, 057601 (2005).
- [61] S. G. Karshenboim, Can. J. Phys. **77**, 241 (1999).
- [62] A. V. Volotka, V. M. Shabaev, G. Plunien and G. Soff, Eur. Phys. J. D **33**, 23 (2005).
- [63] A. Dupays, A. Beswick, B. Lepetit, C. Rizzo, and D. Bakalov, Phys. Rev. A **68**, 052503 (2003).
- [64] M. I. Eides, Phys. Rev. A **53**, 2953 (1996).
- [65] S. J. Brodsky, C. E. Carlson, J. R. Hiller and D. S. Hwang, Phys. Rev. Lett. **94**, 022001 (2005); Phys. Rev. Lett. **94**, 169902 (E) (2005).
- [66] J. L. Friar and I. Sick, Phys. Rev. Lett. **95**, 049101 (2005); S. J. Brodsky, C. E. Carlson, J. R. Hiller and D. S. Hwang, Phys. Rev. Lett. **95**, 049102 (2005).
- [67] G. T. Bodwin and D. R. Yennie, Phys. Rev. D **37**, 498 (1988).
- [68] A. P. Martynenko, Phys. Rev. A **71**, 022506 (2005).
- [69] A. C. Zemach, Phys. Rev. **104**, 1771 (1956).
- [70] P. L. Anthony *et al.* [E155 Coll.], Phys. Lett. B **493**, 19 (2000).
- [71] P. L. Anthony *et al.* [E155 Coll.], Phys. Lett. B **553**, 18 (2003).
- [72] R. Fatemi *et al.* [CLAS Coll.], Phys. Rev. Lett. **91**, 222002 (2003).

- [73] J. Yun *et al.*, Phys. Rev. C **67** 055204, (2003); S. Kuhn, private communication.
- [74] A. Deur, arXiv:nucl-ex/0507022.
- [75] C. K. Iddings, Phys. Rev. **138**, B446 (1965).
- [76] S. D. Drell and J. D. Sullivan, Phys. Rev. **154**, 1477 (1967).
- [77] E. De Rafael, Phys. Lett. B **37**, 201 (1971).
- [78] P. Gnädig and J. Kuti, Phys. Lett. B **42**, 241 (1972).
- [79] R. N. Faustov and A. P. Martynenko, Eur. Phys. J. C **24**, 281 (2002); R. N. Faustov and A. P. Martynenko, Phys. Atom. Nucl. **65**, 265 (2002) [Yad. Fiz. **65**, 291 (2002)].
- [80] V. Nazaryan, C. E. Carlson and K. A. Griffioen, Phys. Rev. Lett. **96**, 163001 (2006).
- [81] S. B. Gerasimov, Sov. J. Nucl. Phys. **2**, 430 (1966) [Yad. Fiz. **2**, 598 (1966)].
- [82] S. D. Drell and A. C. Hearn, Phys. Rev. Lett. **16**, 908 (1966).
- [83] S. Simula, M. Osipenko, G. Ricco and M. Taiuti, Phys. Rev. D **65**, 034017 (2002). Silvano Simula provided us with an updated version of the code, including error estimates.
- [84] R. N. Faustov, I. V. Gorbacheva and A. P. Martynenko, arXiv:hep-ph/0610332.
- [85] S. G. Karshenboim, Phys. Lett. **225A**, 97 (1997).
- [86] J. L. Friar and I. Sick, Phys. Lett. B **579**, 285 (2004).
- [87] P. J. Mohr and B. N. Taylor, Rev. Mod. Phys. **72**, 351 (2000); and Rev. Mod. Phys. **77**, 1 (2005) [2002 CODATA]; *Cf.*, the electron scattering value of I. Sick, Phys. Lett. B **576**, 62 (2003) or the spread from Sick's value to that of J. J. Kelly, Phys. Rev. C **70**, 068202 (2004).
- [88] D. Drechsel, B. Pasquini and M. Vanderhaeghen, Phys. Rept. **378**, 99 (2003).
- [89] P. Pedroni [GDH and A2 Coll.], AIP Conf. Proc. **814**, 374 (2006); H. Dutz *et al.* [GDH Coll.], Phys. Rev. Lett. **94**, 162001 (2005).
- [90] D. A. Dicus and R. Vega, Phys. Lett. B **501**, 44 (2001).
- [91] G. Altarelli, N. Cabibbo and L. Maiani, Phys. Lett. B **40**, 415 (1972).
- [92] H. D. I. Abarbanel and S. Nussinov, Phys. Rev. **158**, 1462 (1967).
- [93] M. Damashek and F. J. Gilman, Phys. Rev. D **1**, 1319 (1970); C. A. Dominguez, C. Ferro Fontan and R. Suaya, Phys. Lett. B **31**, 365 (1970).
- [94] S. J. Brodsky, F. E. Close and J. F. Gunion, Phys. Rev. D **8**, 3678 (1973).
- [95] A. Antognini *et al.*, AIP Conf. Proc. **796**, 253 (2005).
- [96] R. N. Faustov, E. V. Cherednikova and A. P. Martynenko, Nucl. Phys. A **703**, 365 (2002).

- [97] A. De Rujula, J.M. Kaplan, and E. de Rafael, Nucl. Phys. **B 53**, 545 (1973).
- [98] S.P. Wells *et al.* (SAMPLE Coll.), Phys. Rev. C **63**, 064001 (2001).
- [99] F. E. Maas *et al.* (A4 Coll.), Phys. Rev. Lett. **94**, 082001 (2005).
- [100] L. Kaufmann (on behalf of Happex Coll.), proceedings PAVI06.
- [101] L. Capozza (on behalf of A4 Coll.), proceedings PAVI06.
- [102] K. Kumar (on behalf of E-158 Coll.), proceedings PAVI06.
- [103] S.K. Phillips, P. King (G0 Coll.), DNP meeting Oct 25-28 2006, Nashville TN, paper HC.00013
- [104] A. Afanasev, I. Akusevich, and N.P. Merenkov, hep-ph/0208260.
- [105] M. Gorchtein, P. A. M. Guichon and M. Vanderhaeghen, Nucl. Phys. A **741**, 234 (2004).
- [106] R. Tarrach, Nuovo Cimento A **28**, 409 (1975).
- [107] L. Diaconescu and M. J. Ramsey-Musolf, Phys. Rev. C **70**, 054003 (2004)
- [108] B. Pasquini and M. Vanderhaeghen, Phys. Rev. C **70**, 045206 (2004).
- [109] D. Drechsel, O. Hanstein, S. Kamalov, and L. Tiator, Nucl. Phys. **A645**, 145 (1999).
- [110] A. V. Afanasev and N. P. Merenkov, Phys. Lett. B **599**, 48 (2004); for corrected formulas and corrected numerical results see also [arXiv:hep-ph/0407167].
- [111] M. Gorchtein, Phys. Rev. C **73**, 035213 (2006); Phys. Rev. C **73**, 055201 (2006).
- [112] M. Gorchtein, Phys. Lett. B **644**, 322 (2007).
- [113] JLab experiment E-05-015, spokespersons T. Averett, J.P. Chen, X. Jiang.
- [114] V. Tvaskis *et al.*, Phys. Rev. C **73**, 025206 (2006)
- [115] J. Arrington, V.F. Dimitriev, R.J. Holt, D.M. Nikolenko, L.A. Rachev, Yu.V. Sheshtakov, V.N. Stibunov, D.K. Toporkov, H. de Vries; Proposal for experiment at VEPP-3, nucl-ex/0408020.
- [116] V. Pascalutsa, C. E. Carlson and M. Vanderhaeghen, Phys. Rev. Lett. **96**, 012301 (2006).
- [117] J. Bartels, Nucl. Phys. B **82**, 172 (1974).
- [118] R. L. Kingsley, Nucl. Phys. B **46**, 615 (1972); P. M. Fishbane and R. L. Kingsley, Phys. Rev. D **8**, 3074 (1973).
- [119] G. T. Bodwin and C. D. Stockham, Phys. Rev. D **11**, 3324 (1975).
- [120] W. J. Marciano and A. Sirlin, Phys. Rev. D **27**, 552 (1983); Phys. Rev. D **29**, 75 (1984) [Erratum-ibid. D **31**, 213 (1985)].
- [121] M. Bohm and H. Spiesberger, Nucl. Phys. B **294**, 1081 (1987).